Mon. Not. R. Astron Soc. **260,** 343–364 (1993)

Phase instability and non-linearity in the distorted dipole pulsation mode of the rapidly oscillating Ap star HR 3831 (HD 83368)

D. W. Kurtz,[1] A. Kanaan[2] and Peter Martinez[1]

[1] *Department of Astronomy, University of Cape Town, Rondebosch 7700, South Africa*
[2] *Instituto de Fisica, Universidade Federal do Rio Grande do Sul, 90049 Porto Alegre-RS, Brazil*

Accepted 1992 July 6. Received 1992 June 12; in original form 1992 February 19

ABSTRACT

HR 3831 is a rapidly oscillating A7p SrCrEu star with $T_{\rm eff} = 8000$ K, $R = 1.9\ R_\odot$, $M_V = 2.0$, $V = 6.168$, $d \approx 60$ pc, a magnetic field which ranges from about -720 $G \leq B_{\rm eff} \leq +780$ G with the rotation period of 2.851982 d, and a pulsation period near 700 s. In this paper, new high-speed photometric observations obtained during 101 h in 1990 and 167 h in 1991 are presented. The 1991 observations were obtained contemporaneously from the South African Astronomical Observatory and Cerro Tololo Inter-American Observatory over a time-span of 17 d with a 41 per cent duty cycle. A frequency analysis of the 1991 data shows that HR 3831 pulsates in a single mode which is rotationally modulated, giving rise to a fundamental frequency septuplet, a first harmonic quintuplet, a second harmonic triplet, and a probable detection of a single frequency at the third harmonic. The fundamental frequency septuplet is shown to be adequately described by a sum of axisymmetric spherical harmonics with $\ell = 0$, 1, 2 and 3. By far, the dominant component of the sum is the dipole, which is why we call the mode a distorted dipole. By comparing the new 1990 and 1991 data with previous data sets obtained in 1981, 1985 and 1986, it is shown that the form of this distorted dipole probably changes slightly from year to year. It is also shown that the phase of the pulsation is variable from year to year, and that this variability cannot be modelled simply by a periodic Doppler shift, caused by an orbital companion, plus a quadratic evolutionary term. The first harmonic quintuplet has changed substantially in form between the 1986 and 1990 data sets. HR 3831 shows a π-radian reversal of its pulsation phase at the two magnetic quadratures. This reversal is not well defined for one quadrature; whether this is because of errors in the observations, or is a physical effect in the star, is not yet known. The relative amplitudes of the second harmonic frequencies remain problematic.

Key words: stars: chemically peculiar – stars: individual: HR 3831 – stars: oscillations.

1 INTRODUCTION

1.1 Basic data

HR 3831 (HD 83368) is a bright ($V = 6.168$) southern peculiar A star classified Ap SrEuCr by Houk (1978), who remarks on the strong Sr lines. It is a visual binary with a separation of 3.29 arcsec and a difference in brightness of $\Delta V = 2.84$ between the components, according to Hurly & Warner (1983), who obtained UBV photometry for the resolved components using an area scanner. They found that, for HR 3831A, $V = 6.25$, $B - V = 0.25$ and $U - B = 0.12$; and for HR 3831B, $V = 9.09$, $B - V = 0.64$ and $U - B = 0.15$. (Note that HR 3831 generally means HR 3831A in this paper. When this is not clear from the context, we shall specify which component we mean.)

From its colours, HR 3831B is close to being a solar analogue, presumably less than 10^9 yr old since, as we will show below, HR 3831A is a main-sequence A star. If we assume that HR 3831B is a G2V star 0.3 mag fainter than the Sun (because of its relative youth), then M_V(HR 3831B) = 5.0 and $d = 66$ pc. Given the potential for error in this estimate, it is consistent with the parallax of $\pi = 0.021$ arcsec (Hoffleit & Jaschek 1982).

At 66 pc, the current linear separation of the two components is at least 217 au. For the sake of argument, let us take that to be the major axis of the orbit. Let us also take the

mass of HR 3831A to be $M_1 = 2\ M_\odot$ and that of HR 3831B to be $M_2 = 1\ M_\odot$. The orbital period is then $P_{orb} = 653$ yr. If the orbit is circular, then HR 3831 has an orbital velocity of about 3 km s^{-1}, or $v/c = 10^{-5}$. For a 653-yr orbit, the radial velocity could change by a maximum factor of $dv/v(\max) = 2\pi(dt/P_{orb}) = 0.01$ in 1 yr, so that any period (including a pulsation period) could show in 1 yr a maximum $dP/P \approx 0.01 \times 10^{-5} \approx 10^{-7}$ [$cP/cP_0 = \lambda/\lambda_0 = 1 + v/c$; $dP/P_0 = dv/c = (dv/v)(v/c)$] from the visual orbit alone. We do not argue that we have given a reasonable description of the orbit of HR 3831; we cannot do that. We have simply shown that the possibility of a changing Doppler shift exists at the level of 1 part in 10^7. This must be kept in mind for the discussion of the long-term behaviour of the phase of the principal pulsation frequency.

Strömgren and Hβ indices have been measured for the unresolved binary system by Martinez (in preparation), who finds $V = 6.168$, $b-y = 0.159$, $m_1 = 0.230$, $c_1 = 0.766$ and $\beta = 2.825$ with errors of about 0.006 mag. If we sum the intensities derived from Hurly & Warner's V measurements of the components ($V_A = 6.25$ and $V_B = 9.09$), we find $V_{A+B} = 6.17$, in exact agreement with the composite measurement of Martinez of $V = 6.168$. We calculate that $B - V = 0.22$ for HR 3831A, after removing the slight reddening caused by the companion. The $b-y$ and β indices must also be slightly reddened by the contribution of the companion to the composite indices.

From $\beta = 2.825$, we find, from the calibration of Moon & Dworetsky (1985), that $T_{eff} = 8000$ K (essentially independent of the luminosity of HR 3831). Hence, if we take HR 3831B to be a G2V star of $M_{bol} = 5.0$, $T_{eff} = 5800$ K and $R = 0.9\ R_\odot$, then we calculate $R = 1.9 \pm 0.1\ R_\odot$ and $M_{bol} = 1.92$ for HR 3831A. (We have taken the bolometric correction to be 0.2 mag for HR 3831A and 0.05 mag for HR 3831B, the error in T_{eff} to be ± 200 K and the error in V to be ± 0.01 mag.) From Crawford's (1979) calibration, we find that $\Delta M_V = 0.7$ mag. Hence the photometry indicates that HR 3831A is an A7V star lying 0.7 mag above the zero-age main sequence (ZAMS).

The Strömgren index, δc_1, is generally not a reliable luminosity index for the Ap stars; line blanketing reduces its numerical value compared to normal stars of the same luminosity. HR 3831 is a good case of this. The δc_1 calculated from Crawford's calibration is $\delta c_1 = -0.062$ which, taken at face value, indicates that HR 3831 lies about 0.5 mag *below* the ZAMS. Thus the δc_1 index underestimates the luminosity of HR 3831 by about 1.2 mag.

HR 3831 is a magnetic variable. The effective magnetic field has been measured nine times by Thompson (1983) and 12 times by Mathys (1991). HR 3831 also varies in brightness with its rotation, presumably because of spots or rings of enhanced rare earth abundance about, or near, the magnetic poles. We refer to these brightness variations as *mean light variations* to distinguish them from the short time-scale pulsational light variations which are the principal focus of this paper.

Kurtz et al. (1992) have analysed the mean light variations and reanalysed the magnetic variations to find that the rotation period of HR 3831 is $P_{rot} = 2.851982 \pm 0.000005$ d, and that the magnetic field varies about a zero-point of 16 ± 42 G with an amplitude of 760 ± 60 G. The spots which produce the mean light variability are not concentric with the magnetic poles, but lag behind them in rotational longitude by 0.055 ± 0.011 of a rotation period.

HR 3831 has a magnetic field which reverses polarity about a mean which is indistinguishable from zero. For a purely dipolar field, $\tan i \tan \beta = (1-r)/(1+r)$, where i is the rotational inclination, β is the magnetic obliquity and $r = B_{eff}(\min)/B_{eff}(\max)$ (where r is restricted to the range $-1 \le r \le +1$). Thus we find, for HR 3831, that $r = -0.96 \pm 0.13$; this indicates that either i or $\beta > 62°$ at the 3σ confidence level. Carney & Peterson (1985) measured the rotational velocity of HR 3831 to be $v \sin i = 33 \pm 3$ km s^{-1}. From our calculation of the radius of HR 3831, $R = 1.9 \pm 0.1\ R_\odot$, and the rotational period, $P_{rot} = 2.851982$ d, we find $v_{rot} = 34 \pm 3$ km s^{-1}. This requires that $i > 38°$ at the 3σ confidence level.

To summarize, HR 3831 is an A7p SrCrEu magnetic star with an effective temperature of $T_{eff} = 8000 \pm 200$ K, a radius of $R = 1.9 \pm 0.1\ R_\odot$ and an absolute magnitude of $M_{bol} = 2.0 \pm 0.3$, where the quoted errors are estimates. It has a polarity-reversing magnetic field which ranges from about +780 G to −720 G with the rotation period of $P_{rot} = 2.851982 \pm 0.000005$ d. From $v \sin i = 33 \pm 3$ km s^{-1} and our radius estimate, $i > 38°$. The magnetic field variations require that either i or $\beta > 62°$. Mean light variations occur with the rotation period, but have extrema which lag behind the magnetic extrema. HR 3831 is a visual binary with a separation of 3.29 arcsec; the secondary is a main-sequence G2 star. From the absolute magnitude of the secondary and from the parallax, we estimate the distance to be about 60 pc.

1.2 The rapid oscillations

HR 3831 is a singly periodic rapidly oscillating Ap (roAp) star which pulsates with a frequency of $\nu = 1.4280128$ mHz ($P = 700.27$ s $= 11.67$ min). Observed through a Johnson B filter, the semiamplitude of the light variation associated with the pulsation ranges from a little over 4 mmag at the times of magnetic extrema to zero at one of the magnetic quadratures [this paper; Kurtz 1990; Kurtz, Shibahashi & Goode (hereafter KSG) 1990; Kurtz & Shibahashi (hereafter KS) 1986; Kurtz 1982]. The amplitude modulation period is the same as the rotation period, $P_{rot} = 2.851982$ d, and the times of pulsation amplitude maxima coincide with the magnetic extrema (Kurtz et al. 1992).

Fig. 1 shows the entire amplitude modulation repertory of HR 3831 in a low-resolution light curve covering the entire time-span of the 1991 data, which will be analysed in Section 3 of this paper. Fig. 2 is a high-resolution light curve of one of the nights shown in Fig. 1, JD 2448313, which allows a detailed look at the pulsation behaviour of this star. The non-sinusoidal character of the variations is apparent in Fig. 2.

HR 3831 is the best studied of the rapidly oscillating Ap (roAp) stars. Recent reviews of these stars are given by Matthews (1991), Kurtz (1990) and Shibahashi (1987). The amplitude modulation of the light curves of the roAp stars can be described by two models: the oblique pulsator model and the spotted pulsator model. The oblique pulsator model assumes that the pulsation and magnetic axes are aligned and are oblique to the rotation axis; the rotation modulation of the light variations is caused by the varying viewing aspect of non-radial pulsation modes (Kurtz 1982; Dziembowski &

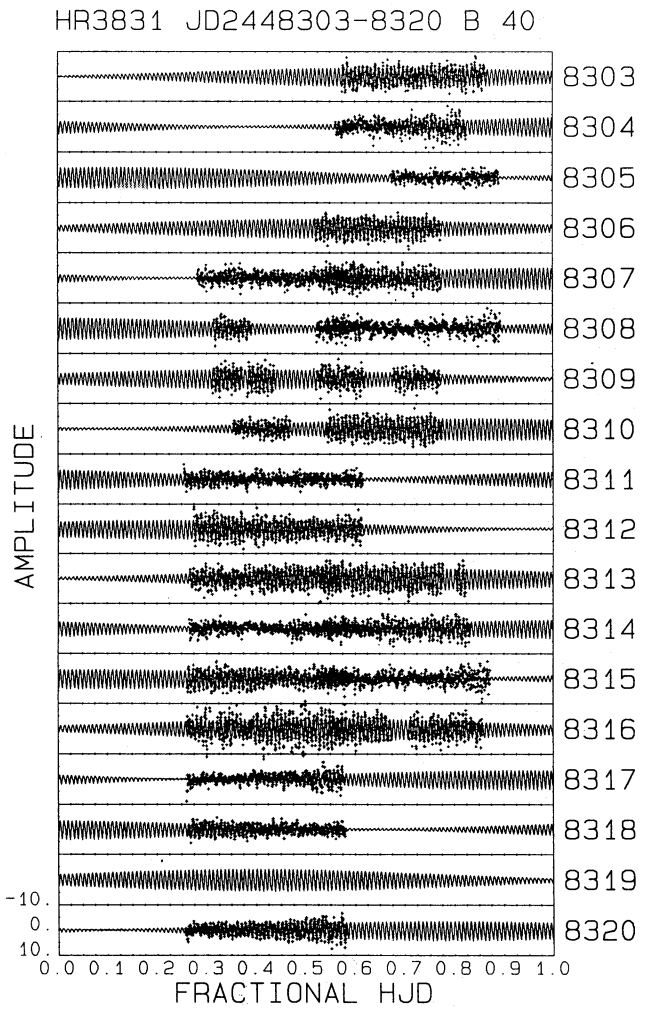

Figure 1. This is a low-resolution light curve of all of the 1991 multi-site high-speed photometric data for HR 3831 with the best-fitting frequency solution discussed in Section 3. Table 1 gives a journal of the data plotted in this figure. Each panel covers a full 24 h in Heliocentric Julian Date, and is 20 mmag high. The number to the right of each panel is HJD − 2440000. The fitted curve shows the amplitude modulation continuously for 17 d; the data points show the 41 per cent duty cycle of this data set. It is difficult at this low resolution to see how well the data points are fitted by the curve – that is shown in detail in Fig. 2.

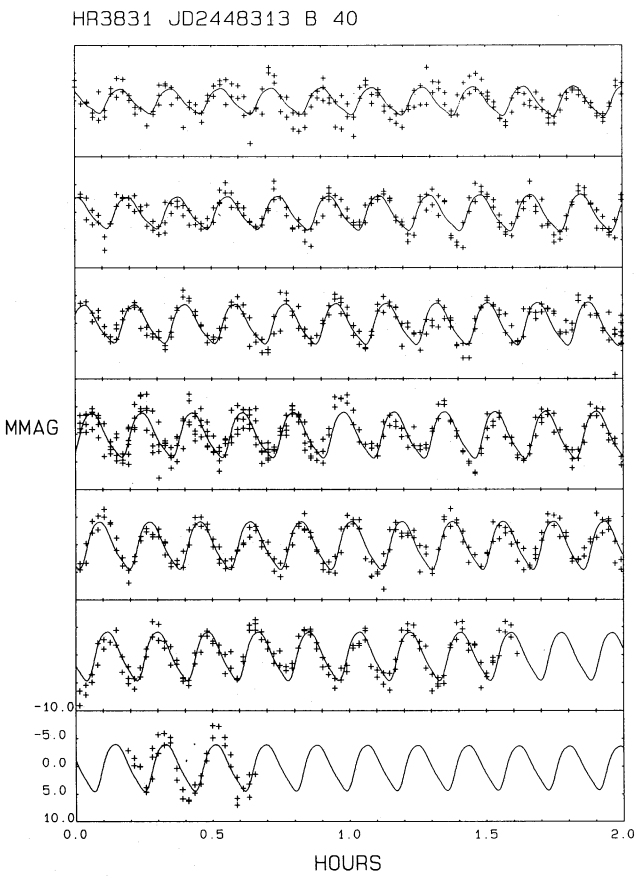

Figure 2. A high-resolution light curve of the JD 2448313 data. Each panel is 2 h long and 20 mmag high. The panels read like lines of print; this is a nearly continuous 12.6-h long light curve. The quality of the fit of the curve to the data and the quality of the data themselves are *typical*; some nights are better, some worse. These are the same data and fit shown in the 8313 panel of Fig. 1.

Goode 1985; KS 1986; Shibahashi 1986; KSG 1990; Kurtz 1990). The spotted pulsator model assumes that the pulsation axis coincides with the rotation axis of the star so that the pulsation modes are always seen from the same viewing angle, but that the ratio of flux to radius variations, f, and the phase lag between the flux and radius variations, ψ, are variable over the surface as a function of the magnetic field strength (Mathys 1985), leading to the observed amplitude modulation. The spotted pulsator model was developed by Mathys to avoid the problem in the oblique pulsator model of the Coriolis Force causing the oblique pulsation axis to drift with respect to the magnetic axis. In the oblique pulsator model, it is assumed that the magnetic perturbation to the pulsation frequency is greater than the Coriolis perturbation causing the pulsation axis to lock to the magnetic axis (Dziembowski & Goode 1985; KS 1986; Shibahashi 1986; Kurtz 1990). Kurtz et al. (1992) have shown that, in HR 3831, the pulsation pattern is in phase with the magnetic field variations and slightly out of phase with the mean light variations. This rules out a spotted pulsator model where variations in f and ψ are functions of the spots associated with the mean light variations, but it does not rule out a spotted pulsator model where f and ψ vary with the magnetic field strength.

In principle, the oblique pulsator model and the spotted pulsator model can be distinguished by radial velocity observations: the oblique pulsator model will show radial velocity modulation, whereas the spotted pulsator model will not. Matthews et al. (1988) found radial velocity amplitude modulation in the roAp star HR 1217, which they concluded favoured the oblique pulsator model. However, HR 1217 is multiperiodic, so the possibility that the radial velocity amplitude modulation was caused by beating among these independent pulsation frequencies was not completely ruled out. This problem could be resolved by high-accuracy radial velocity measurements of HR 3831. Judging from the variations in HR 1217, the peak-to-peak radial velocity amplitude in HR 3831 is probably of the order of several hundred m s^{-1}; at $V=6.17$, measurements accurate enough to study this variation with good signal-to-noise ratio are possible.

We will assume the oblique pulsator model throughout the rest of this paper.

1.3 The dipole character of the pulsation mode in HR 3831

Previous studies of HR 3831 have shown that this star pulsates in a single mode which is basically dipolar with the pulsation axis and magnetic axis aligned. Fig. 3 shows the evidence for this, using the 1991 data presented in this paper. It can be seen that the pulsation amplitude is modulated with two maxima per rotation and a π-radian phase reversal at the times of magnetic quadrature.

These quadratures can be calculated from the magnetic field measurements. It is easy to show, for a dipole field, that the phase of quadrature is given by

$$\cos \Theta_{quad} = -1/\tan i \tan \beta = -(1+r)/(1-r), \quad (1)$$

where Θ_{quad} is the rotational phase (in cycles) measured from the time of magnetic maximum. For $r = -0.96 \pm 0.13$, equation (1) gives $\Theta_{quad} = 0.253$ and 0.747 (± 0.012) cycles. Fig. 3 shows that these are the times of the phase reversal in HR 3831.

The pulsation mode in HR 381 is not purely a dipole mode – it is a distorted dipole. KSG (1990) discussed the problem of this distortion. They noted that their analysis of the 1981–86 data for HR 3831 showed more frequencies in the amplitude spectrum than just the frequency triplet associated with the oblique dipole mode, and they noted that the central frequency of the dipole frequency triplet did not have the same phase as the other two members of the triplet as is required in the oblique pulsator model for a pure dipole mode. They suggested that more observations were

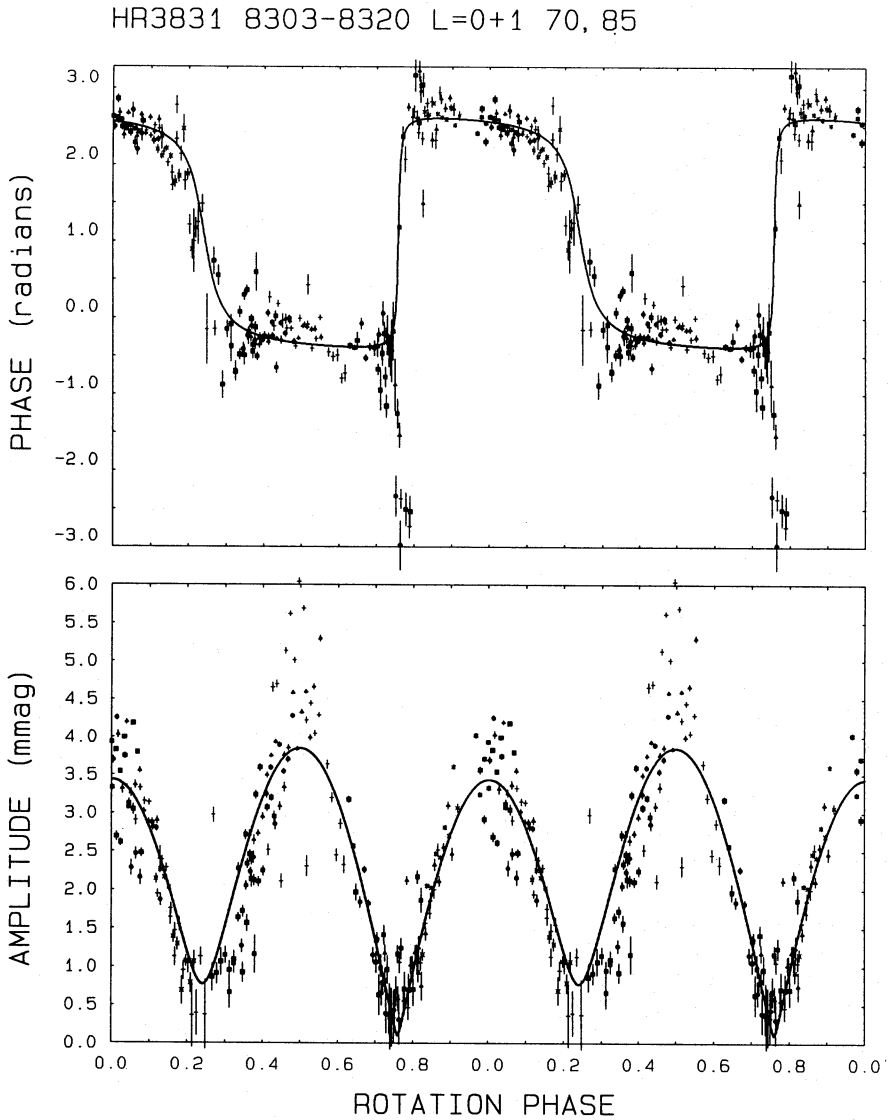

Figure 3. This diagram plots the pulsation phase and amplitude as a function of the rotation phase for HR 3831. The rotation phase is calculated from the time of magnetic maximum using the ephemeris given by Kurtz et al. (1992) with the rotation period $P_{rot} = 2.851982$ d; two rotation cycles are plotted. Each point in the diagram has been calculated by fitting the frequency $\nu = 1.4280128$ mHz to four cycles (46.685 min) of the high-speed photometric data by linear least-squares. The solid lines show the best fit to the frequencies derived in Section 3 assuming a pulsation mode which can be described by the sum of $\ell = 0$ and 1 spherical harmonics, a rotational inclination of $i = 70°$ and a magnetic obliquity of $\beta = 85°$. See Kurtz (1992) for the derivation of the fitting procedure.

necessary to determine those additional frequencies, and to unravel the mystery of the phase of the central frequency. They were also unable to provide a physical model for the amplitude spectra of the first and second harmonics.

The curves in Fig. 3 are theoretical fits to the data for a distorted dipole mode with both dipole and radial components under the assumptions of the oblique pulsator model (KSG 1990; KS 1986). The radial component is necessary to account for the phase of the central peak of the frequency triplet. The fitting procedure is discussed more fully in Section 5, and derived by Kurtz (1992) in detail. It can be seen in Fig. 3 that the pulsation in HR 3831 cannot be described with only dipole plus radial components. Note that the fitted curve does not describe the phase reversal at the $\Theta = 0.747$ quadrature, and it does not fit the amplitude-modulation curve well. We shall return to these problems in Section 5.

Heller & Kawaler (1988) predicted, from models of A stars, that evolutionary frequency changes may be observable in roAp stars with observations spanning as little as a decade, given the photometric accuracy achieved for stars like HR 3831. To search for evolutionary frequency changes, a stable, well-resolved pulsation frequency must be found and monitored. HR 3831, with its apparently single pulsation mode, seems a good candidate for such a study.

For this reason, and to resolve the dipole-distortion problems which KSG were unable to explain, we have obtained 268 h of new high-speed photometric observations of HR 3831 in 1990 and 1991. This paper presents these observations, their frequency analysis and our interpretaton of the results of this analysis.

2 NEW PHOTOMETRIC OBSERVATIONS

New high-speed photometric observations of HR 3831 were obtained in 1990 February, March and May and in 1991 February. The 1991 observations were obtained using the 0.6-m telescope of Cerro Tololo Inter-American Observatory (CTIO) and the 1.0-m telescope of the South African Astronomical Observatory (SAAO) contemporaneously. The observations were obtained through Johnson *B* filters using continuous 10-s integrations with occasional interruptions for sky brightness measurements. They were corrected for coincidence losses, sky background and excitation while the times were corrected to Heliocentric Julian Date (HJD) to an accuracy of 10^{-5} d. Some low-frequency filtering was performed and the observations were averaged to produce 40-s integrations.

Table 1 gives a journal of the new observations. Listed are the civil date of the observations, the Heliocentric Julian Date of the first 40-s integration, the number of 40-s integrations obtained, the time-span of each observing run in hours, the standard deviation of the data with respect to the mean for the run, the telescope used and the observer. The standard deviations listed include all sources of noise plus the actual variation of HR 3831.

3 FREQUENCY ANALYSIS OF THE 1991 DATA

The 1991 data listed in Table 1 span almost exactly 17 d = 408 h, during which nearly 167 h of observations were obtained, giving a duty cycle of 41 per cent. This is very good for a data set obtained from only two observing sites. Fig. 1 shows the time distribution of the data. These data also have lower noise than previous data sets. We shall see later in this paper that we do not currently understand the behaviour of the pulsation phase in HR 3831 over long time-spans, and hence we cannot combine the data sets in different years for a successful high-resolution frequency analysis. For these reasons, we analyse the 1991 data set alone here.

The frequency analysis was performed using a faster algorithm (Kurtz 1985) based on Deeming's (1975) discrete Fourier transform (DFT). Individual Fourier transforms were computed for short sections of the 1991 data where the frequency resolution required is low, in order to avoid the accumulation of computer truncation error, which arises in the faster algorithm when tens of thousands of frequencies are calculated. The low-resolution Fourier transforms were then interpolated to higher frequency resolution and co-added with correct phase and weighting factors (O'Donoghue 1981; O'Donoghue & Warner 1982) to produce amplitude spectra. We prefer the amplitude spectrum to the power spectrum because it allows a direct comparison with the light curves.

Fig. 4 shows the entire amplitude spectrum of the 1991 data almost out to the Nyquist frequency (12.5 mHz for 40-s data). Although the fine details are compressed by the scale of this diagram, 60 000 frequencies are calculated with a

Table 1. Journal of new observations of HR 3831.

Date	HJD_{start} 2440000.+	n	t hr	σ mmag	tel	obs
1990						
Feb 06/07	7929.48704	282	3.21	1.78	SAAO 1.0-m	PM
Feb 08/09	7931.35161	588	6.75	3.10	SAAO 1.0-m	PM
Feb 10/11	7933.27887	652	8.49	1.63	SAAO 1.0-m	PM
Feb 11/12	7934.29758	714	8.06	3.18	SAAO 1.0-m	PM
Feb 16/17	7939.27405	332	7.96	1.41	SAAO 1.0-m	DWK
Mar 06/07	7957.26676	245	2.94	3.27	SAAO 1.0-m	DWK
Mar 07/08	7958.25538	659	7.40	2.98	SAAO 1.0-m	DWK
Mar 08/09	7959.25735	670	7.48	1.24	SAAO 1.0-m	DWK
Mar 09/10	7960.25354	597	7.51	2.41	SAAO 1.0-m	DWK
Mar 10/11	7961.25401	712	7.97	3.10	SAAO 1.0-m	DWK
Mar 11/12	7962.25494	642	7.18	1.70	SAAO 1.0-m	DWK
Mar 12/13	7963.25112	683	7.66	1.51	SAAO 1.0-m	DWK
May 04/05	8016.24234	275	3.60	1.21	SAAO 0.75-m	PT
May 05/06	8017.25278	242	2.92	2.66	SAAO 0.75-m	PT
May 06/07	8018.23342	358	4.08	3.17	SAAO 0.75-m	PT
May 09/10	8021.20886	114	1.35	2.97	SAAO 1.0-m	DWK
May 10/11	8022.20210	383	4.36	1.57	SAAO 1.0-m	DWK
May 11/12	8023.20137	76	0.86	1.74	SAAO 1.0-m	DWK
May 12/13	8024.19670	136	1.55	2.83	SAAO 1.0-m	DWK
Σ		8360	101.33			
1991						
Feb 15/16	8303.57449	574	6.93	2.88	CTIO 0.6-m	AK
Feb 16/17	8304.56144	553	6.33	2.41	CTIO 0.6-m	AK
Feb 17/18	8305.67489	450	5.19	1.50	CTIO 0.6-m	AK
Feb 18/19	8306.52016	526	6.06	2.87	CTIO 0.6-m	AK
Feb 19/20	8307.28164	728	8.33	2.05	SAAO 1.0-m	PM
	8307.53234	505	5.77	2.47	CTIO 0.6-m	AK
Feb 20/21	8308.31627	345	3.92	2.29	SAAO 1.0-m	PM
	8308.54462	739	8.40	2.00	SAAO 1.0-m	PM
Feb 21/22	8309.31339	241	3.02	3.17	SAAO 1.0-m	PM
	8309.52231	398	4.60	2.88	CTIO 0.6-m	AK
Feb 22/23	8310.35520	228	2.72	1.93	SAAO 1.0-m	PM
	8310.54258	485	5.59	3.05	CTIO 0.6-m	AK
Feb 23/24	8311.25429	754	8.68	1.60	SAAO 1.0-m	PM
Feb 24/25	8312.27410	711	8.16	2.98	SAAO 1.0-m	PM
Feb 25/26	8313.26636	637	7.26	2.85	SAAO 1.0-m	PM
	8313.52886	572	7.06	3.42	CTIO 0.6-m	AK
Feb 26/27	8314.26447	678	7.65	1.65	SAAO 1.0-m	DWK
	8314.54184	610	6.94	2.35	CTIO 0.6-m	AK
Feb 27/28	8315.26044	687	7.73	2.37	SAAO 1.0-m	DWK
	8315.52102	738	8.42	2.08	SAAO 1.0-m	DWK
Feb 28/29	8316.26050	654	7.63	4.14	SAAO 1.0-m	DWK
	8316.54812	574	7.43	3.31	CTIO 0.6-m	AK
Mar 01/02	8317.25902	676	7.61	1.83	SAAO 1.0-m	DWK
Mar 02/03	8318.26292	673	7.60	1.65	SAAO 1.0-m	DWK
Mar 04/05	8320.25489	696	7.84	2.13	SAAO 1.0-m	DWK
Σ		14432	166.87			

resolution of 0.0002 mHz – more than sufficient for a 17-d time-span data set. This figure clearly shows the presence of the fundamental, first and second harmonics of the pulsation in HR 3831. We shall argue that the third harmonic is also detected, even though it is not convincing in this diagram. The apparent peak near 8.4 mHz is an artefact of a 2-min drive error and small sensitivity drifts as a function of the position of HR 3831 within a 30-arcsec observing diaphragm with the SAAO 0.75-m telescope *only*. We emphasize that this peak is not present in data obtained with the SAAO 1-m and the CTIO 0.6-m telescopes, so it is definitely an artefact.

Fig. 4 shows that the noise level is a function of frequency. The highest noise peaks are around 0.12 mmag for the low-frequency end of the spectrum and about 0.05 mmag at the high-frequency end. For the lowest frequencies, $\nu < 0.6$ mHz, the noise level would be higher but for our filtering at these low frequencies. Above 0.6 mHz, the noise drops as the dominant noise source changes from sky transparency variations to scintillation. Because the noise is not exactly white, and because these error estimates depend on the total variance in the data, our *internal* error estimates in amplitude and phase, in both linear least-squares and non-linear least-squares fits, will be too low for the low-frequency end of the spectrum and too high for the high-frequency end.

We shall divide the rest of this section into subsections in which we study, for higher resolution amplitude spectra, the fundamental frequencies, the first harmonic frequencies, the second harmonic frequencies and the third harmonic frequency, respectively. The procedure we shall use in each subsection is as follows. We identify the highest peak in the amplitude spectrum and fit to the data the frequency associated with that peak, first by linear least-squares and then by non-linear least-squares. The optimized frequency, amplitude and phase so determined are then removed in the time domain from the light curves, and the next-highest peak is searched for. We refer to this procedure as 'pre-whitening'. For the second, and all subsequent, frequencies found, all frequencies are fitted simultaneously in the linear least-squares and non-linear least-squares fitting procedures.

The following subsections contain a detailed discussion of the frequency analysis of the 1991 data. We consider the detail of the discussion to be important for a realistic estimate of the errors and pitfalls in the analysis. Those who wish to assess the final adopted frequencies critically will find this section indispensable; others may wish to skip to the discussion of the results in Section 4.

3.1 The fundamental frequencies in the 1991 data

Fig. 5 is a high-resolution amplitude spectrum of the 1991 data in the frequency range 1.33 mHz$\leq\nu\leq$1.53 mHz showing all of the frequencies associated with the fundamental pulsation mode of HR 3831 convolved with their

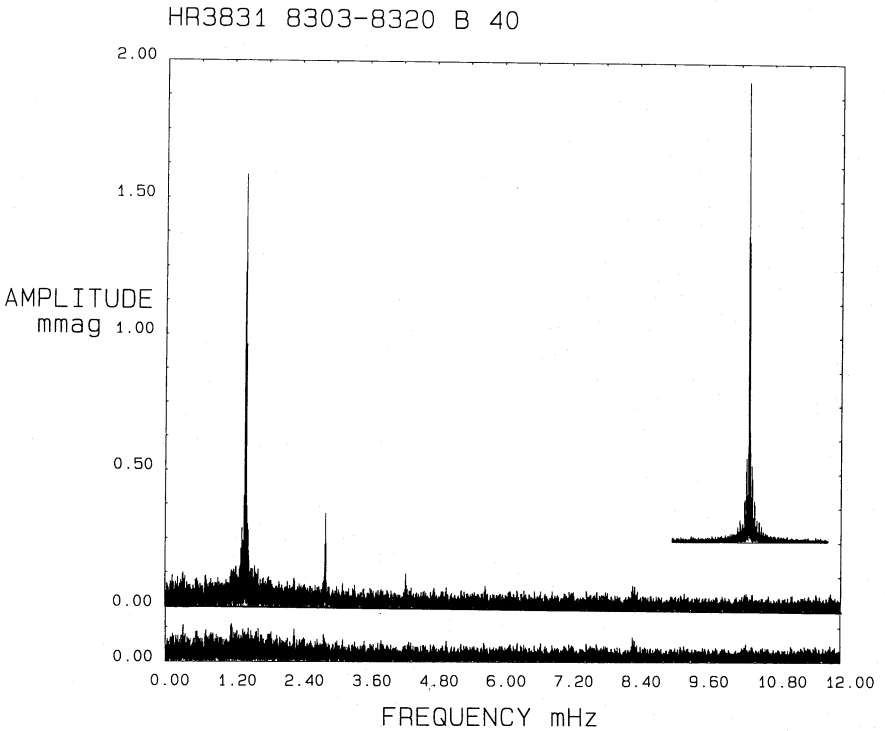

Figure 4. A low-resolution amplitude spectrum of the 1991 data. There are 60 000 frequencies plotted here with a frequency resolution of 0.0002 mHz – sufficient to resolve all peaks in the spectrum. The fundamental frequencies cluster around 1.428 mHz, the first harmonic frequencies around 2.856 mHz, and the second harmonic frequencies around 4.284 mHz. Those peaks stand unequivocally above the noise. A third harmonic peak is also present, near 5.712 mHz, which we claim is real (see Fig. 13 for a higher resolution look at this peak). However, the peaks at 8.4 mHz are artefacts of a 2-min drive error in the SAAO 0.75-m telescope. See the text for arguments in favour of the reality of the 5.712-mHz peak and against the reality of the 8.4-mHz peak. The inset shows the central section of the spectral window for these data at the same scale as the amplitude spectrum itself. The lower panel shows the noise level after the frequency solution given in Table 2 has been removed from the data. Note the decrease in noise as a function of frequency.

spectra windows. The highest peak, ν_1, is easily resolved. Fig. 6 shows the spectral window, which was produced by sampling a noise-free sinusoid with the frequency and amplitude of the highest peak in Fig. 5 at the actual times of observation of the 1991 data. Because the data were obtained at two sites separated by 6 h of longitude, the 1 d^{-1} aliases are not a problem and the 2 d^{-1} and higher aliases are nearly non-existent.

The highest peak in Fig. 5 is

$\nu_1 = 1.423964 \pm 0.000005$ mHz,
$A_1 = 1.908 \pm 0.025$ mmag, $\phi_1 = -3.060 \pm 0.013$ rad,

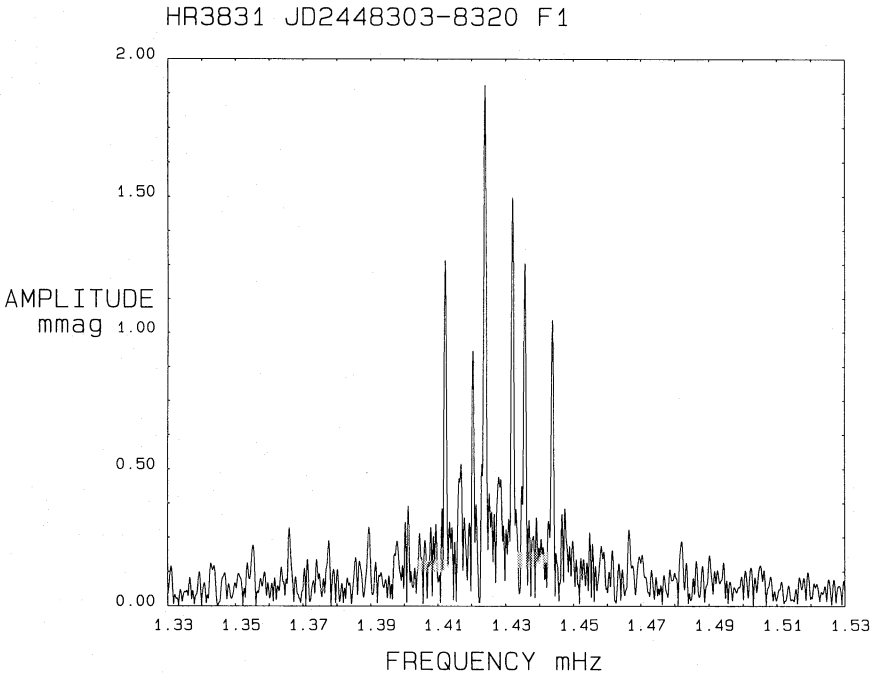

Figure 5. A high-resolution amplitude spectrum of the 1991 data in the frequency range 1.33–1.53 mHz. The highest peak is $\nu_1 = 1.423964$ mHz.

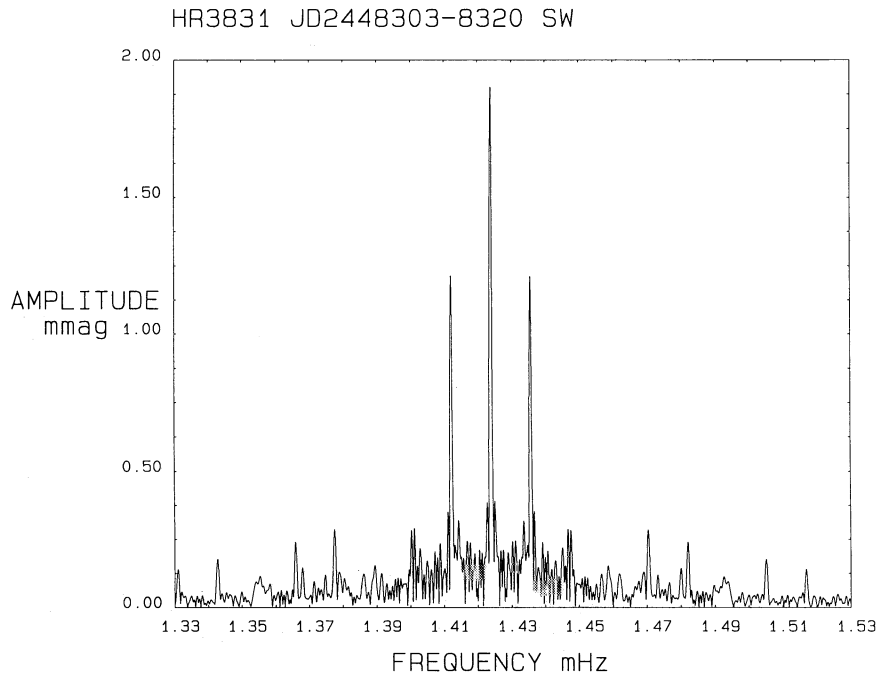

Figure 6. The spectral window for the 1991 data at the same scale as Fig. 5. The spectral window has been calculated by sampling a noise-free sinusoid with the frequency and amplitude of the highest peak in Fig. 5 at the actual times of observation of the 1991 data.

where t_0 = HJD 2448312.241 is the time of magnetic maximum (Kurtz et al. 1992) here and throughout Section 3. For a data set with well-resolved frequencies and many cycles of data, Fourier analysis and least-squares fitting give identical results. This can be seen for ν_1 where we find $A_1 = 1.904$ mmag (DFT), $A_1 = 1.907 \pm 0.025$ mmag (linear least-squares) and $A_1 = 1.908 \pm 0.025$ mmag (non-linear least-squares); the phases determined by all three methods are indistinguishable.

After pre-whitening the data by ν_1, we find the next highest peak at $\nu_2 = 1.43210$ mHz, which is shown in Fig. 7. Simultaneous non-linear least-squares fitting of ν_1 and ν_2 gives

$\nu_1 = 1.4239517 \pm 0.0000044$ mHz,
$A_1 = 1.972 \pm 0.022$ mmag, $\phi_1 = -2.993 \pm 0.011$ rad,

$\nu_2 = 1.4321126 \pm 0.0000056$ mHz,
$A_2 = 1.575 \pm 0.022$ mmag, $\phi_2 = -2.994 \pm 0.014$ rad.

Comparing this two-frequency fit with the one-frequency fit, there are several points to note.

(i) The errors for both the amplitude and phase have been reduced. This is because those errors depend on the total variance in the data; the two-frequency fit reduces that variance more than does the one-frequency fit.

(ii) The amplitude A_1 has changed by nearly 3σ between the two fits. This is because of interference between the spectral windows of the two frequencies; the real and imaginary parts of the Fourier transform add in complex space, so such interference can increase, or decrease, the amplitude determined for individual frequencies when compared with simultaneous fits for multiple frequencies. This warns us to take care when using internal errors solely determined from the least-squares fits; systematic errors caused by interference between determined frequencies, and from unresolved frequencies, may be larger than the nominal internal errors.

(iii) The optimized value for the frequency of ν_1 has also shifted by nearly 3σ between the one-frequency and two-frequency fits. Again, this warns us to be aware of possible systematic errors.

(iv) The phases of ν_1 and ν_2 are equal: $\phi_1 = \phi_2$. Thus we can see already that the two highest amplitude frequencies in the 1991 HR 3931 data reach maximum constructive interference with each other at the time of magnetic maximum.

The top panel of Fig. 8 shows the amplitude spectrum of the residuals after pre-whitening by ν_1 and ν_2. The highest peak here is $\nu_3 = 1.42792$ mHz. Simultaneous non-linear least-squares fitting of ν_1, ν_2 and ν_3 gives

$\nu_1 = 1.4239514 \pm 0.0000044$ mHz,
$A_1 = 1.977 \pm 0.021$ mmag, $\phi_1 = -2.994 \pm 0.011$ rad,

$\nu_2 = 1.4321171 \pm 0.0000054$ mHz,
$A_2 = 1.586 \pm 0.021$ mmag, $\phi_2 = -2.984 \pm 0.013$ rad,

$\nu_3 = 1.4279251 \pm 0.0000168$ mHz,
$A_3 = 0.518 \pm 0.021$ mmag, $\phi_3 = 1.381 \pm 0.041$ rad.

These three frequencies are similar to those which have been found in previous studies of HR 3831, where they have been interpreted to be the components of an oblique dipole mode (KS 1986; KSG 1990; Kurtz 1990). From the above, $\nu_3 - \nu_1 = 3.97 \pm 0.02$ μHz and $\nu_2 - \nu_3 = 4.19 \pm 0.02$ μHz; from Kurtz et al. (1992), $\nu_{rot} = 4058.256 \pm 0.007$ nHz. Although $\nu_3 - \nu_1$ and $\nu_2 - \nu_3$ differ from ν_{rot} within their internal errors, the full width at half maximum of the peaks in the amplitude spectra for the 1991 data is $\sigma = 0.2$ μHz. Since the internal errors are applicable only if no unresolved frequencies are present, for the moment we shall assume that ν_1, ν_2 and ν_3 are separated by ν_{rot}.

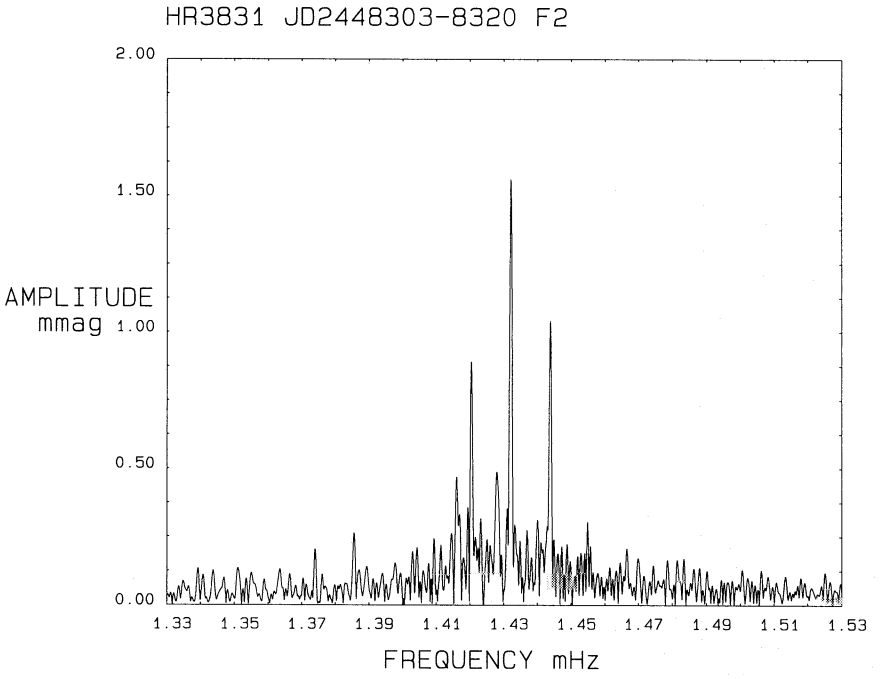

Figure 7. A high-resolution amplitude spectrum of the residuals after pre-whitening by ν_1. The highest peak here is $\nu_1 = 1.43210$ mHz.

The second panel of Fig. 8 shows the amplitude spectrum of the residuals after pre-whitening by ν_1, ν_2 and ν_3. The highest peak here is $\nu_4 = 1.41565$ mHz. Although this peak looks as if it could be confused with others, we note that it does not occur at a random frequency: $\nu_1 - 2\nu_{rot} = 1.41583$ mHz. Within the 0.2-μHz resolution of the data set, $\nu_4 = \nu_1 - 2\nu_{rot}$.

By comparing the second and fourth panels of Fig. 8, we take the amplitude signal-to-noise ratio to be about 3 for ν_4. The False Alarm probability of finding a peak of this amplitude is $F = 1-(1-e^{-z})^N$ (Horne & Baliunas 1986), where z is the signal-to-noise ratio in power ($z = 9$ in this case) and N is the number of independent Fourier frequencies searched. However, we do not want to determine the chance of finding a $z = 9$ peak *anywhere* in Fig. 8, because ν_4 lies at a *particular* frequency, namely one of the rotational sidelobes of ν_2. If we say that we would have identified any frequency which coincided with $\nu_2 \pm 2\nu_{rot}$ or $\nu_2 \pm 3\nu_{rot}$ or their $\pm 1\ d^{-1}$ aliases, then $N = 12$ and the chance of finding a $z = 9$ peak is only $F = -(1-e^{-9})^{12} = 0.001$. There is little chance that ν_4 is not real.

Simultaneous non-linear least-squares fitting of ν_1 to ν_4 gives

$\nu_1 = 1.4239541 \pm 0.0000044$ mHz,
$A_1 = 2.003 \pm 0.024$ mmag, $\phi_1 = -2.992 \pm 0.013$ rad,

$\nu_2 = 1.4321248 \pm 0.0000054$ mHz,
$A_2 = 1.572 \pm 0.024$ mmag, $\phi_2 = -2.989 \pm 0.013$ rad,

$\nu_3 = 1.4280294 \pm 0.0000225$ mHz,
$A_3 = 0.475 \pm 0.024$ mmag, $\phi_3 = 1.174 \pm 0.041$ rad,

$\nu_4 = 1.4158068 \pm 0.0000401$ mHz,
$A_4 = 0.272 \pm 0.024$ mmag, $\phi_4 = -2.193 \pm 0.094$ rad.

Note that the error estimate for the amplitude has increased from the three-frequency fit, indicating some interference of the window patterns of the frequencies. For ν_3, the shift in frequency relative to the three-frequency fit is caused by the poor resolution between ν_4 and $\nu_3 - 1\ d^{-1}$, because $3\nu_{rot} \approx 1\ d^{-1}$. This tends to obscure ν_4 in single-site studies.

The third panel of Fig. 8 shows the amplitude spectrum of the residuals after pre-whitening by ν_1 to ν_4. The highest peak here is $\nu_5 = 1.41986$ mHz. This peak is not convincing. There are several others of similar height and none stands out well above the surrounding noise. However, as with ν_4, we note that ν_5 does not have a random frequency: $\nu_1 - \nu_{rot} = 1.41990$ mHz. Within the 0.2-μHz resolution of the data set, $\nu_5 = \nu_1 - \nu_{rot}$. If we take the amplitude signal-to-noise ratio here to be 2 and now $N = 9$, then $z = 4$ and $F = 0.15$. Obviously this argument is extremely sensitive to our estimate of the signal-to-noise ratio. We think that ν_5 is probably real.

Simultaneous non-linear least-squares fitting of ν_1 to ν_5 gives

$\nu_1 = 1.4239545 \pm 0.0000044$ mHz,
$A_1 = 2.001 \pm 0.026$ mmag, $\phi_1 = -2.990 \pm 0.011$ rad,

$\nu_2 = 1.4320970 \pm 0.0000065$ mHz,
$A_2 = 1.639 \pm 0.026$ mmag, $\phi_2 = -2.998 \pm 0.013$ rad,

$\nu_3 = 1.4280306 \pm 0.0000224$ mHz,
$A_3 = 0.482 \pm 0.026$ mmag, $\phi_3 = 1.165 \pm 0.041$ rad,

$\nu_4 = 1.4158033 \pm 0.0000411$ mHz,
$A_4 = 0.269 \pm 0.026$ mmag, $\phi_4 = -2.227 \pm 0.094$ rad,

$\nu_5 = 1.4199351 \pm 0.0000481$ mHz,
$A_5 = 0.222 \pm 0.026$ mmag, $\phi_5 = 1.723 \pm 0.094$ rad.

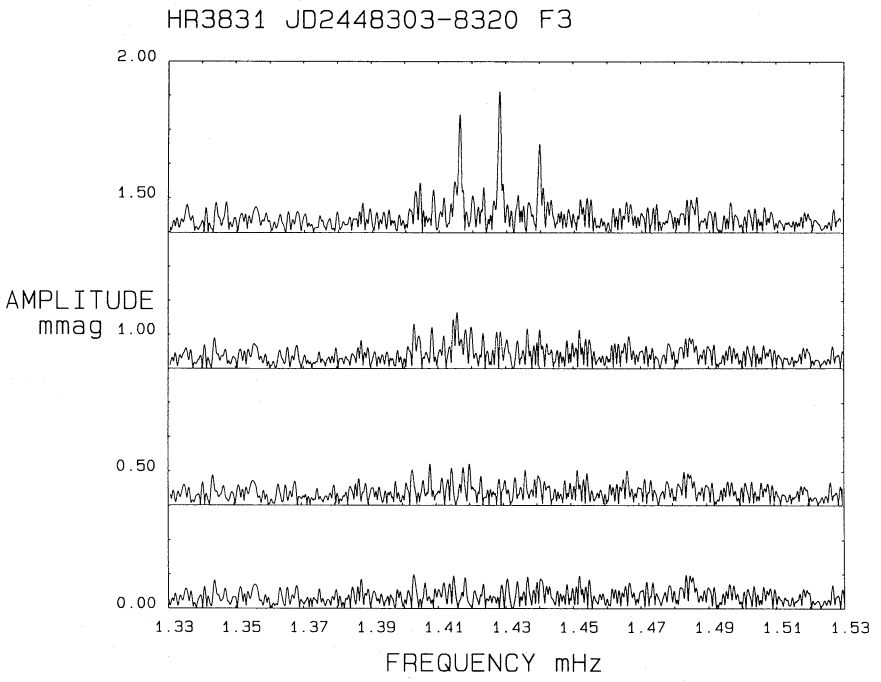

Figure 8. A high-resolution amplitude spectrum showing the pre-whitening steps in the analysis of the fundamental frequencies. The top panel shows $\nu_3 = 1.42792$ mHz in the residuals after ν_1 and ν_2 have been pre-whitened. The second panel shows $\nu_4 = 1.41565$ mHz in the residuals after ν_1–ν_3 have been pre-whitened. The third panel shows $\nu_5 = 1.41986$ mHz in the residuals after ν_1 to ν_4 have been pre-whitened. The bottom panel is taken to be noise. Arguments are given in the text in favour of the reality of ν_4 and ν_5. The zero-point of the ordinate scale is the bottom line of each panel. The scale in all four panels is the same and is given along the ordinate axis.

The bottom panel of Fig. 8 shows the amplitude spectrum of the residuals after pre-whitening by ν_1 to ν_5. This amplitude spectrum is indistinguishable from noise. The highest peaks have amplitudes of 0.12 mmag, which is five times the formal internal error from the non-linear least-squares fit of ν_1 to ν_5. We judge from that that a realistic error estimate for the amplitude determinations would be $\sigma_A = 0.05$ mmag in the frequency range covered by this part of the amplitude spectrum.

Comparing the frequency separations of ν_2 to ν_5 from the highest amplitude frequency ν_1 with the rotation frequency, we find

$(\nu_1 - \nu_4) - 2\nu_{\rm rot} = 34.7 \pm 41.3$ nHz,

$(\nu_1 - \nu_5) - \nu_{\rm rot} = -38.9 \pm 48.3$ nHz,

$(\nu_1 - \nu_3) + \nu_{\rm rot} = -17.8 \pm 22.8$ nHz,

$(\nu_1 - \nu_2) + 2\nu_{\rm rot} = 26.0 \pm 7.8$ nHz.

Within 3.3σ, or less, of the internal frequency errors, this set of frequencies determined from non-linear least-squares fitting is separated by the rotation frequency of HR 3831.

3.2 The first harmonic frequencies in the 1991 data

Fig. 9 is a high-resolution amplitude spectrum of the 1991 data in the frequency range 2.76 mHz$\leq\nu\leq$2.96 mHz showing all of the frequencies associated with the first harmonics of HR 3831 convolved with their spectral windows. The highest peak is $\nu_6 = 2.85610$ mHz. A non-linear least-squares fit of ν_6 to the data gives

$\nu_6 = 2.856092 \pm 0.000030$ mHz,
$A_6 = 0.395 \pm 0.030$ mmag, $\phi_6 = -1.02 \pm 0.08$ rad.

We note that $\nu_6 = 2\nu_3$, which justifies calling the frequencies in this section the first harmonic frequencies. The internal error in amplitude is slightly greater than that given for the fundamental frequencies, even though the noise is lower at these higher frequencies. This is simply because, for the analysis in this section, we have not pre-whitened the fundamental frequencies ν_1 to ν_5 from the data, and hence the total variance includes those frequencies as well as the noise. In the end, we will remove all determined frequencies together so that the final error estimates will include only noise.

The top panel of Fig. 10 shows the amplitude spectrum of the residuals after pre-whitening by ν_6. The highest peak here is $\nu_7 = 2.84813$ mHz. Simultaneous non-linear least-squares fitting of ν_6 and ν_7 gives

$\nu_6 = 2.856097 \pm 0.000030$ mHz,
$A_6 = 0.397 \pm 0.030$ mmag, $\phi_6 = -1.04 \pm 0.08$ rad,

$\nu_7 = 2.848127 \pm 0.000085$ mHz,
$A_7 = 0.143 \pm 0.030$ mmag, $\phi_7 = -1.19 \pm 0.21$ rad.

The second panel of Fig. 10 shows the amplitude spectrum of the residuals after pre-whitening by ν_6 and ν_7. The highest peak here is $\nu_8 = 2.85170$ mHz. Simultaneous non-linear least-squares fitting of ν_6, ν_7 and ν_8 gives

$\nu_6 = 2.856109 \pm 0.000031$ mHz,
$A_6 = 0.398 \pm 0.030$ mmag, $\phi_6 = -1.03 \pm 0.08$ rad,

$\nu_7 = 2.848318 \pm 0.000080$ mHz,
$A_7 = 0.156 \pm 0.030$ mmag, $\phi_7 = -1.20 \pm 0.21$ rad,

$\nu_8 = 2.851698 \pm 0.000101$ mHz,
$A_8 = 0.124 \pm 0.030$ mmag, $\phi_8 = -1.82 \pm 0.24$ rad.

The bottom panel in Fig. 10 shows the amplitude spectrum of the residuals after pre-whitening by ν_6, ν_7 and ν_8. The highest peaks here have amplitudes of 0.09 mmag or less, and are probably noise. It is interesting to note for future

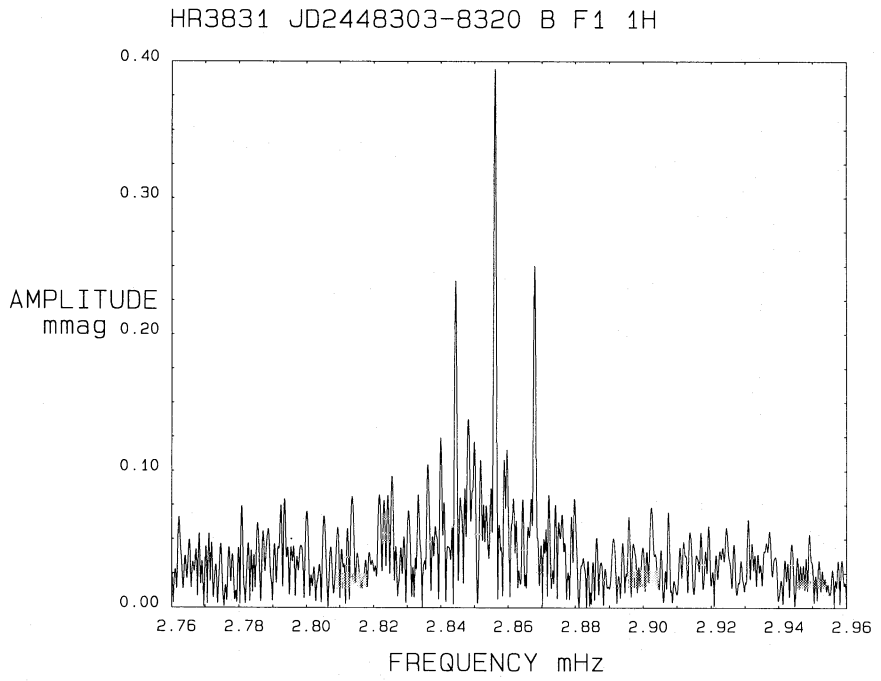

Figure 9. A high-resolution amplitude spectrum of the 1991 data in the frequency range 2.76–1.96 mHz. The highest peak is $\nu_6 = 2.85610$ mHz.

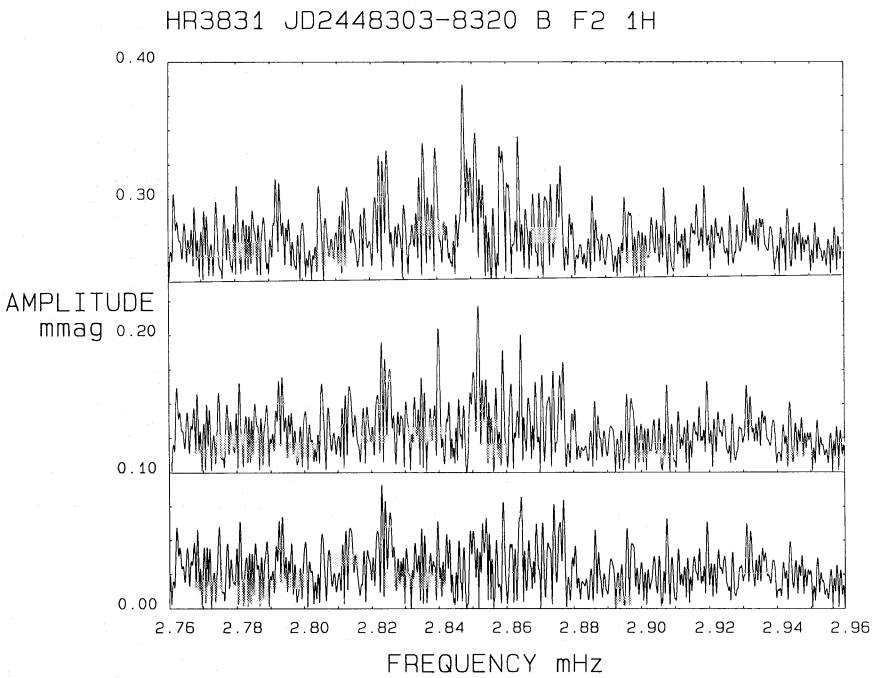

Figure 10. A high-resolution amplitude spectrum showing the pre-whitening steps in the analysis of the first harmonic frequencies. The top panel shows $\nu_7 = 2.84813$ mHz in the residuals after ν_6 has been pre-whitened. The second panel shows $\nu_8 = 2.85170$ mHz in the residuals after ν_6 and ν_7 have been pre-whitened. The bottom panel is taken to be noise, although the second-highest peak lies at $\nu_6 + 2\nu_{\rm rot}$. The zero-point of the ordinate scale is the bottom line of each panel. The scale in all three panels is the same and is given along the ordinate axis.

reference that the second-highest peak has a frequency of 2.86435 mHz which is $\nu_6 + 2\nu_{\rm rot}$.

Comparing the frequency separations of ν_7 and ν_8 from the highest amplitude frequency ν_6 with the rotation frequency, we find

$$(\nu_6 - \nu_8) - \nu_{\rm rot} = 0.35 \pm 0.11\ \mu\text{Hz},$$

$$(\nu_6 - \nu_7) - 2\nu_{\rm rot} = -0.33 \pm 0.09\ \mu\text{Hz}.$$

As with the fundamental frequencies, within 3.7σ, or less, of the internal frequency errors, these final frequencies determined from non-linear least-squares fitting are separated by the rotation frequency of HR 3831.

3.3 The second harmonic frequencies in the 1991 data

Fig. 11 is a high-resolution amplitude spectrum of the 1991 data in the frequency range $4.175\ \text{mHz} \le \nu \le 4.375\ \text{mHz}$ showing all of the frequencies associated with the second harmonics of HR 3831 convolved with their spectral windows. The highest peak is $\nu_9 = 4.28810$ mHz.

A non-linear least-squares fit of ν_9 to the data gives

$$\nu_9 = 4.28810 \pm 0.00009\ \text{mHz},$$
$$A_9 = 0.139 \pm 0.030\ \text{mmag}, \qquad \phi_9 = 2.0 \pm 0.2\ \text{rad}.$$

Note that $\nu_9 = 3\nu_3 + \nu_{\rm rot}$. The top panel of Fig. 12 shows the amplitude spectrum of the residuals after pre-whitening by ν_9. The highest peak here is $\nu_{10} = 4.28000$ mHz. Simultaneous non-linear least-squares fitting of ν_9 and ν_{10} gives

$$\nu_9 = 4.28812 \pm 0.00008\ \text{mHz},$$
$$A_9 = 0.145 \pm 0.030\ \text{mmag}, \qquad \phi_9 = 2.0 \pm 0.2\ \text{rad},$$

$$\nu_{10} = 4.28000 \pm 0.00010\ \text{mHz},$$
$$A_{10} = 0.121 \pm 0.030\ \text{mmag}, \qquad \phi_{10} = 2.1 \pm 0.2\ \text{rad}.$$

The bottom panel of Fig. 12 shows the amplitude spectrum of the residuals after pre-whitening by ν_9 and ν_{10}. The highest peaks here have amplitudes of 0.07 mmag or less, and are indistinguishable from noise.

Comparing the frequency separation of ν_9 and ν_{10} with the rotation frequency, we find

$$(\nu_9 - \nu_{10}) - 2\nu_{\rm rot} = 0.00 \pm 0.13\ \mu\text{Hz}.$$

We also note that $\nu_9 = 3\nu_3 + \nu_{\rm rot}$ and $\nu_{10} = 3\nu_3 - \nu_{\rm rot}$, which justifies calling these frequencies the second harmonic frequencies.

3.4 The third harmonic frequency in the 1991 data

Fig. 13 is a high-resolution amplitude spectrum of the 1991 data in the frequency range $5.612\ \text{mHz} \le \nu \le 5.812\ \text{mHz}$ showing the frequency associated with the third harmonic of HR 3831. The highest peak is at $\nu = 5.70045$ mHz; its $+1\ \text{d}^{-1}$ alias is $\nu_{11} = 5.71221\ \text{mHz} = 4\nu_3$. The signal-to-noise ratio here is not good, so the reality of ν_{11} is arguable. The False Alarm probability for finding a peak of this amplitude depends strongly on our estimate of the real noise. If we take the signal-to-noise ratio for ν_{11} to be 2.5σ in amplitude (6.25σ in power), then $F = 1 - (1 - e^{-z})^N = 0.04$ (Horne & Baliunas 1986), where $z = 6.25$ is the signal-to-noise ratio in power and $N = 21$, given that we would have identified any frequency which coincided with $4\nu_3$ or any of its $\pm\nu_{\rm rot}$, $\pm 2\nu_{\rm rot}$ or $\pm 3\nu_{\rm rot}$ rotational sidelobes, or their $\pm 1\ \text{d}^{-1}$ aliases. Thus we claim that ν_{11} is probably real.

4 DISCUSSION OF THE FREQUENCIES

We saw in the development of the frequency analyses above that interference between the window patterns of the

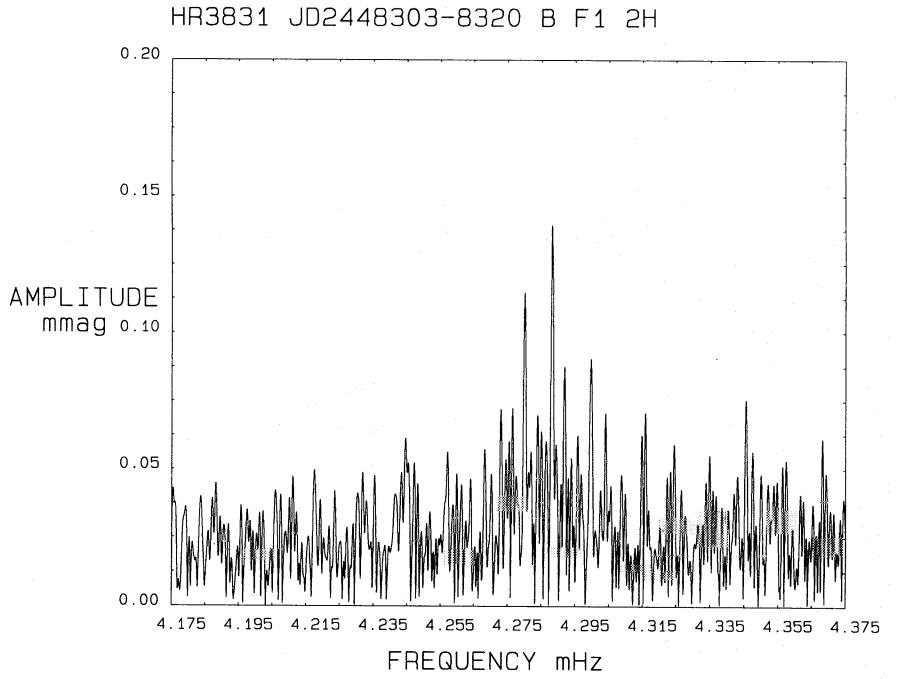

Figure 11. A high-resolution amplitude spectrum of the 1991 data in the frequency range 4.175–4.375 mHz. The highest peak is $\nu_9 = 4.28810$ mHz.

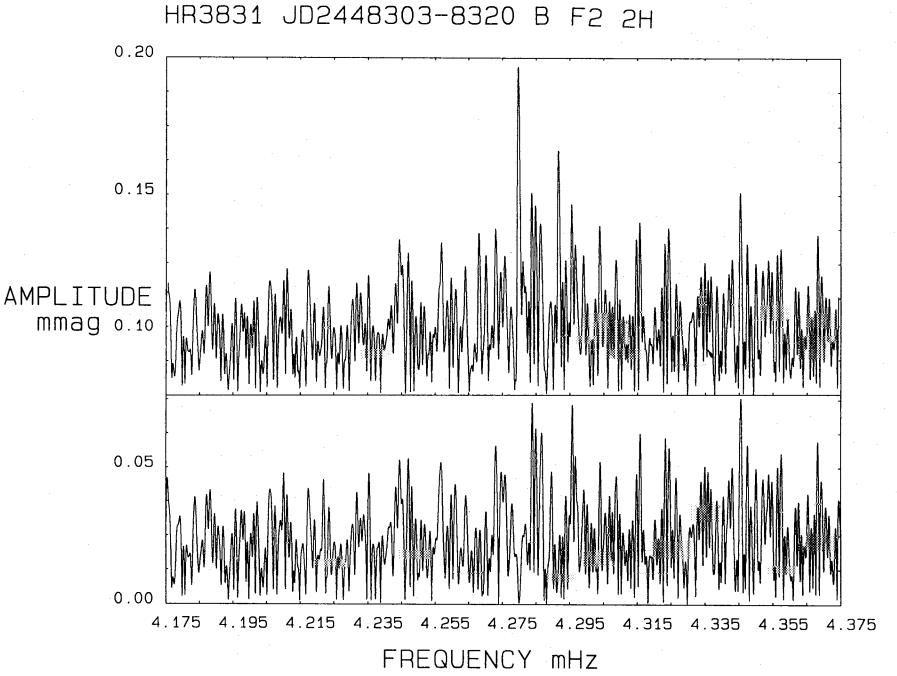

Figure 12. A high-resolution amplitude spectrum showing the pre-whitening steps in the analysis of the second harmonic frequencies. The top panel shows $\nu_{10} = 4.28000$ mHz in the residuals after ν_9 has been pre-whitened. The bottom panel is taken to be noise. The zero-point of the ordinate scale is the bottom line of each panel. The scale in both panels is the same and is given along the ordinate axis.

identified frequencies could, in some cases, shift the frequencies by more than 3σ as new frequencies were added to the non-linear least-squares solutions. We therefore conclude that the formal internal errors in frequency given in the last section are somewhat smaller than the real errors. Given this assumption, there is an obvious pattern to the frequencies: *within the errors, the fundamental frequencies are all separated by the rotation frequency, and the harmonic frequencies are all exact multiples of one of the fundamental frequencies, or separated from such a multiple by the rotation frequency.*

As we saw in Fig. 3, past studies of HR 3831 have shown that the basic frequency pattern indicates an oblique dipole pulsation mode. Our three highest amplitude fundamental

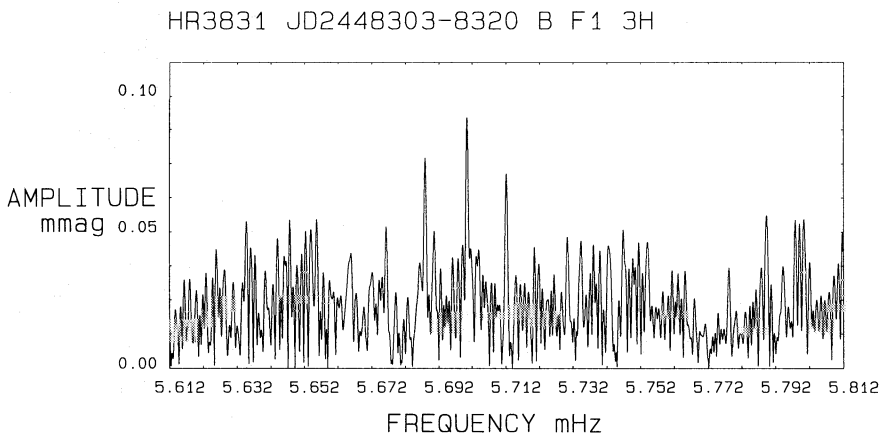

Figure 13. A high-resolution amplitude spectrum of the 1991 data in the frequency range 5.612–5.812 mHz. The highest peak is $\nu = 5.70045$ mHz; its $+1\ \mathrm{d}^{-1}$ alias is $\nu_{11} = 5.71221$ mHz $= 4\nu_3$. We argue in the text that this is probably not an artefact.

frequencies, ν_1, ν_2 and ν_3, continue to fit this interpretation, but with the new, higher accuracy data we can now see that the pulsation mode is more complex than a pure dipole.

We assume here that ν_3 is the actual pulsation mode and that ν_1 and ν_2, the two highest amplitude frequencies, describe the amplitude modulation of ν_3 with rotation. Since ν_1 is the highest amplitude, and hence the best-determined frequency, we start with it and form the following set of frequencies which we fit to the 1991 data set: the principal pulsation frequency is taken to be $\nu = \nu_1 + \nu_{\mathrm{rot}} = 1.4239545$ mHz $+ 0.004058256$ mHz $= 1.4280128$ mHz, where ν_{rot} is taken from Kurtz et al. (1992). We then fit ν and its various rotational sidelobes and harmonics to the 1991 data set with the results given in Table 2. The bottom panel of Fig. 4 shows the noise in the residuals after the frequencies in Table 2 have been pre-whitened from the data. Note that in Table 2 we have made a slight adjustment to t_0 to force the phases of $\nu - \nu_{\mathrm{rot}}$ and $\nu + \nu_{\mathrm{rot}}$ to be equal. This gives $t_0 =$ JD 2448312.24019, which is within 1.5σ of t_0 (pulsational) = JD 2448312.246 ± 0.004 and t_0 (negative magnetic extremum) = JD 2448312.27 ± 0.03 given by Kurtz et al. (1992).

If we then use the linear least-squares results of Table 2 to find a non-linear least-squares fit, we find that the new non-linear least-squares fit changes the frequencies by less than 1σ in each case. Thus we can get a consistent solution to the light variations of HR 3831 of the form given in Table 2 within the final internal errors. Only the assumption that the frequencies are separated by *exactly* ν_{rot} biases this result.

4.1 The amplitudes of the fundamental frequencies

Fig. 14 shows a schematic amplitude spectrum of a linear least-squares fit of the frequency nonuplet ν, $\nu \pm \nu_{\mathrm{rot}}$, $\nu \pm 2\nu_{\mathrm{rot}}$, $\nu \pm 3\nu_{\mathrm{rot}}$ and $\nu \pm 4\nu_{\mathrm{rot}}$ to the 1991 data. The horizontal line shows the height of the highest noise peaks in the bottom panel of Fig. 8. The five frequencies which stand above this level are just ν_1 to ν_5, which we identified in Section 3.1, adjusted to be separated by exactly ν_{rot}. Note that $\nu + 3\nu_{\mathrm{rot}}$ is nearly as high as the highest peaks in the noise of the residuals; we suggest that it is probably real and not an artefact, even though we could not find it in an unbiased analysis of the frequencies.

Table 2. A least-squares fit of $\nu = 1.4280128$ mHz and its rotational sidelobes and harmonics to the 1991 data set.

Frequency name	Frequency mHz	Amp mmag	Phase rad
$\nu - 3\nu_{\mathrm{rot}}$	1.4158380	0.243±0.022	-3.0430±0.0904
$\nu - 2\nu_{\mathrm{rot}}$	1.4198962	0.267±0.022	1.1426±0.0811
$\nu - \nu_{\mathrm{rot}}$	1.4239545	1.974±0.022	2.6014±0.0110
ν	1.4280128	0.481±0.023	0.5805±0.0483
$\nu + \nu_{\mathrm{rot}}$	1.4320710	1.640±0.022	2.6013±0.0133
$\nu + 2\nu_{\mathrm{rot}}$	1.4361293	0.085±0.022	0.0084±0.2549
$\nu + 3\nu_{\mathrm{rot}}$	1.4401875	0.126±0.022	-2.9291±0.1742
$2\nu - 2\nu_{\mathrm{rot}}$	2.8479090	0.113±0.022	-2.4037±0.1918
$2\nu - \nu_{\mathrm{rot}}$	2.8519673	0.128±0.022	2.7427±0.1698
2ν	2.8560255	0.404±0.021	-2.3549±0.0511
$2\nu + \nu_{\mathrm{rot}}$	2.8600838	0.054±0.022	1.3846±0.4032
$2\nu + 2\nu_{\mathrm{rot}}$	2.8641420	0.121±0.022	-2.3580±0.1788
$3\nu - \nu_{\mathrm{rot}}$	4.2799800	0.121±0.020	-0.0447±0.1698
3ν	4.2840383	0.064±0.021	-2.2201±0.3200
$3\nu + \nu_{\mathrm{rot}}$	4.2880965	0.144±0.020	-0.1701±0.1426
4ν	5.7120510	0.065±0.023	1.7344±0.3163

$t_0 =$ HJD 2448312.24019, $\sigma = 1.7386$ mmag per observation.

Previous studies of HR 3831 (Kurtz 1982; KS 1986; KSG 1990) only identified $\nu - \nu_{\mathrm{rot}}$, ν and $\nu + \nu_{\mathrm{rot}}$, whereas we have also identified $\nu - 2\nu_{\mathrm{rot}}$, $\nu - 3\nu_{\mathrm{rot}}$ and probably $\nu + 3\nu_{\mathrm{rot}}$. We must determine whether the amplitude modulation of ν has changed since the previous studies, causing these new frequencies to appear, or whether they were present in the earlier data, but not detected because of a lower signal-to-noise ratio.

To do this we have fitted the same frequencies given in Table 2 to four previous data sets: the data obtained from JD 2444577–4735 (Kurtz 1982), from JD 2446136–6150 (KS 1986), from JD 2446501–6514 (KSG 1990) and from JD 2447931–7963 (this paper, Table 1). (The fit for the JD 2446136–6150 data has too much interference between the window patterns of ν, $\nu - 3\nu_{\mathrm{rot}}$ and $\nu + 3\nu_{\mathrm{rot}}$ because of the sparsity of the observations in that data set, so we omit it

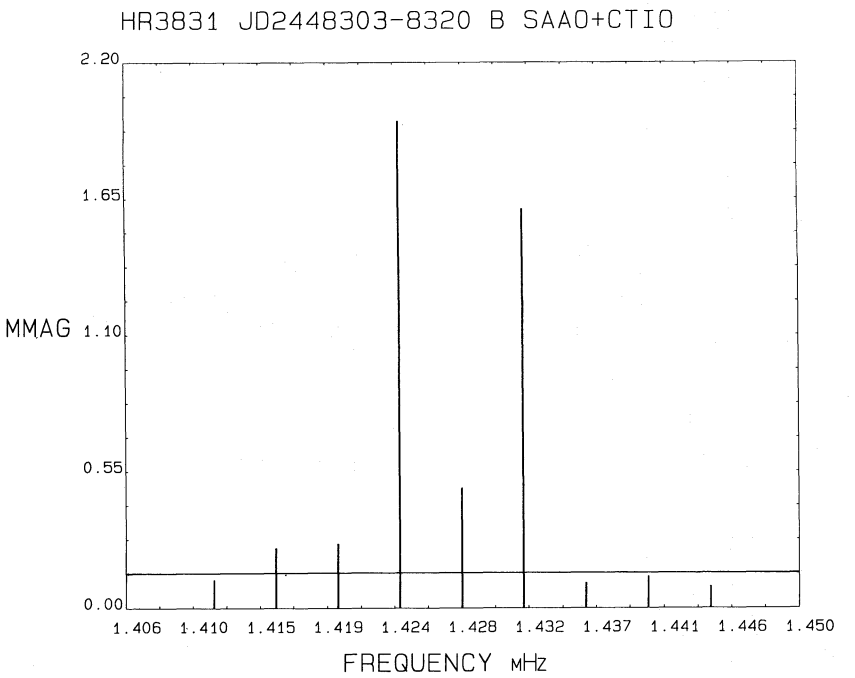

Figure 14. A schematic amplitude spectrum for the fundamental frequencies showing a linear least-squares fit of the frequency nonuplet ν, $\nu \pm \nu_{rot}$, $\nu \pm 2\nu_{rot}$, $\nu \pm 3\nu_{rot}$ and $\nu \pm 4\nu_{rot}$ to the 1991 data.

from the following discussion.) The results for the amplitudes are given in Table 3 and shown graphically in a schematic amplitude spectrum in Fig. 15.

There have been small, but statistically significant (within the internal errors) changes in the amplitudes from year to year – particularly noticeable for the amplitude of $\nu + \nu_{rot}$. We suggest that these changes are probably real. We shall lend further support to this argument in the next section and in the interpretation in Section 5.

However, our basic conclusion is that the form of the amplitude modulation of the fundamental mode with rotation has changed only slightly over the 3743-d (10-yr) time-span of the observations. This is an important conclusion which will bear strongly on our discussion of the phase of the fundamental pulsation mode in Section 5.

4.2 The amplitudes of the first harmonic frequencies

Table 3 shows the amplitudes derived for the first harmonic frequencies for the various data sets. Here there has been a highly significant change of amplitude in some of the component frequencies of the first harmonic.

For the 1981 (JD 2444577–4735), 1985 (JD 2446136–6150) and 1986 (JD 2446501–6514) data, the amplitude of the 2ν frequency is 0.40 mmag with the $2\nu - 2\nu_{rot}$ and $2\nu + 2\nu_{rot}$ frequencies each having half this amplitude, 0.20 mmag, within the errors. The $2\nu - \nu_{rot}$ and $2\nu - \nu_{rot}$ frequencies have no significant amplitude in these data sets. On the other hand, the 1990 (JD 2447931–7963) and 1991 (JD 2448303–8320) data show the 2ν frequency with the same amplitude as in the previous data sets, 0.40 mmag, but now the $2\nu - \nu_{rot}$ and $2\nu - 2\nu_{rot}$ both have amplitudes of about 0.12 mmag; the $2\nu + 2\nu_{rot}$ frequency has a similar amplitude

Table 3. A least-squares fit of $\nu = 1.4280128$ mHz and its rotational sidelobes and harmonics to four data sets.

Frequency name	Frequency mHz	A mmag	B mmag	C mmag	D mmag
		±0.026	±0.036	±0.029	±0.023
$\nu - 3\nu_{rot}$	1.4158380	0.161	0.194	0.176	0.243
$\nu - 2\nu_{rot}$	1.4198962	0.209	0.121	0.310	0.267
$\nu - \nu_{rot}$	1.4239545	2.080	1.954	2.034	1.974
ν	1.4280128	0.443	0.459	0.500	0.481
$\nu + \nu_{rot}$	1.4320710	1.710	1.528	1.787	1.640
$\nu + 2\nu_{rot}$	1.4361293	0.153	0.070	0.082	0.085
$\nu + 3\nu_{rot}$	1.4401875	0.097	0.087	0.075	0.126
$2\nu - 2\nu_{rot}$	2.8479090	0.191	0.180	0.104	0.113
$2\nu - \nu_{rot}$	2.8519673	0.061	0.043	0.172	0.128
2ν	2.8560255	0.443	0.383	0.449	0.404
$2\nu + \nu_{rot}$	2.8600838	0.013	0.027	0.053	0.054
$2\nu + 2\nu_{rot}$	2.8641420	0.159	0.140	0.088	0.121
$3\nu - \nu_{rot}$	4.2799800	0.051	0.039	0.039	0.121
3ν	4.2840383	0.049	0.073	0.030	0.064
$3\nu + \nu_{rot}$	4.2880965	0.112	0.110	0.114	0.144
4ν	5.7120510	0.045	0.032	0.086	0.065

A = JD 2444577-4735, B = JD 2446501-6514, C = JD 2447931-7963, D = JD 2448303-8320 and t_0 = JD 2448312.24012.

in the forced fit of Table 3, but was not independently detected in the frequency analysis of Section 3.2.

All of this is shown graphically in a schematic amplitude spectrum in Fig. 16. The 1990 data cover the entire rotation cycle of HR 3831, as can be seen in Fig. 3; the 1981, 1986 and 1990 data sets have reasonable rotation coverage (KS

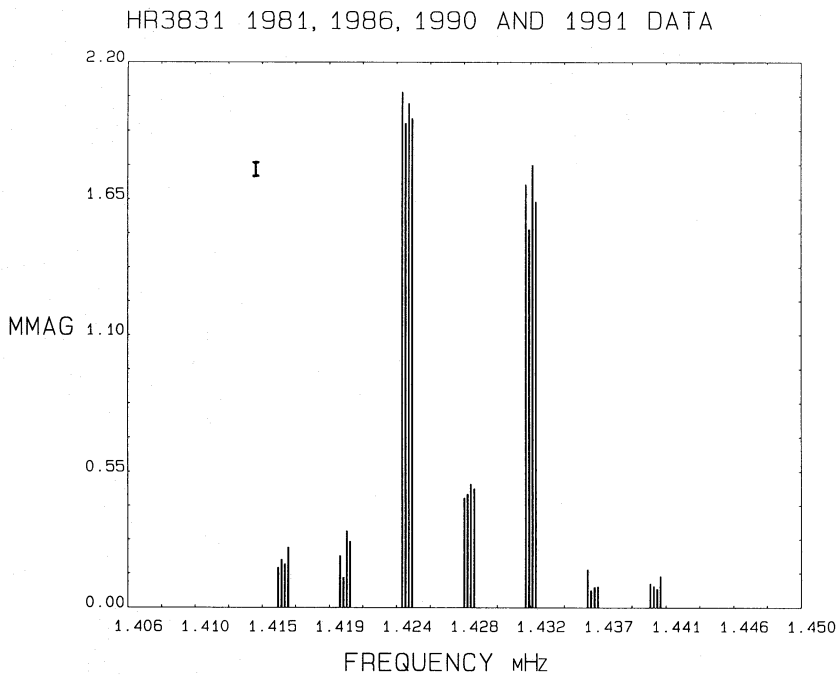

Figure 15. A schematic amplitude spectrum for the fundamental frequencies showing a linear least-squares fit of the frequency septuplet ν, $\nu \pm \nu_{rot}$, $\nu \pm 2\nu_{rot}$ and $\nu \pm 3\nu_{rot}$ to four data sets: JD 2444577–4735 (1981), JD 2446501–6514 (1986), JD 2447931–7963 (1990) and JD 2448303–8320 (1991). We have shifted the amplitude spectrum for each data set by a small frequency to display all four sets on the same diagram. At each frequency the left peak is 1981, the second peak 1986, the third 1990 and the right peak is 1991. The separation of the four components in frequency is for display only; all four peaks coincide. The left peak is actually plotted at the correct frequency. We suggest that some of the apparent variation in the amplitudes of the components is real, but that the basic form of the rotational amplitude modulation has remained the same for 10 yr. The error bar is ± 0.05 mmag, which is twice the internal error; in the text, we estimate that this is more realistic for these low frequencies.

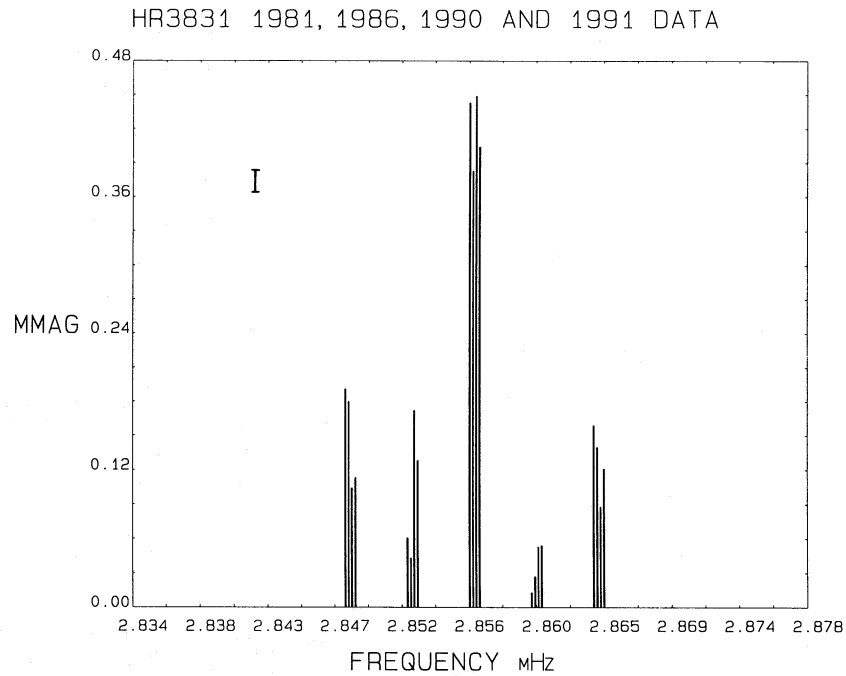

Figure 16. A schematic amplitude spectrum for the first harmonic frequencies showing a linear least-squares fit of the frequency quintuplet 2ν, $2\nu \pm \nu_{rot}$ and $2\nu \pm 2\nu_{rot}$ to four data sets: JD 2444577–4735 (1981), JD 2446501–6514 (1986), JD 2447931–7963 (1990) and JD 2448303–8320 (1991). We have shifted the amplitude spectrum for each data set by a small frequency to display all four sets on the same diagram. At each frequency the left peak is 1981, the second peak 1986, the third 1990 and the right peak is 1991. The separation of the four components in frequency is for display only; all four peaks coincide. The left peak is actually plotted at the correct frequency. The amplitudes are significantly different for the different data sets. The length of the 1σ error bar is 0.02 mmag.

1986; KSG 1990; Kurtz 1990); Figs 18, 20 and 21 show this (see later). Thus the change in the form of the amplitude modulation of the first harmonic does not appear to be an artefact of incomplete sampling of the rotation cycle – it appears to be a real effect of the pulsation of the star.

Table 4. The $\ell = 0+1+2+3$ fit to the frequencies of HR 3831 given in Table 1 for $i = 70°$, $\beta = 70°$.

$A_{-3}(\ell)$ mmag	$A_{-2}(\ell)$ mmag	$A_{-1}(\ell)$ mmag	$A_0(\ell)$ mmag	$A_{+1}(\ell)$ mmag	$A_{+2}(\ell)$ mmag	$A_{+3}(\ell)$ mmag	$\phi(\ell)$ rad	ℓ
0.243	0.178	0.027	0.146	0.022	0.116	0.126	-3.043	3
	0.388	0.341	0.200	0.247	0.200		0.736	2
		2.075	0.501	1.709			2.752	1
			0.864				-0.054	0

The change in the amplitudes of the first harmonic frequencies from year to year lends credibility to our suggestion that the amplitudes of the fundamental frequencies are also variable.

4.3 The amplitudes of the second and third harmonic frequencies

One of the second harmonic frequencies, $3\nu + \nu_{rot}$, was detected in the 1986 data by KSG (1990). In Section 3.3, we showed that both $3\nu - \nu_{rot}$ and $3\nu + \nu_{rot}$ are present in the 1991 data. The signal-to-noise ratio is poor for these frequencies because of their low amplitude, so it is not possible to say whether their amplitudes have been constant

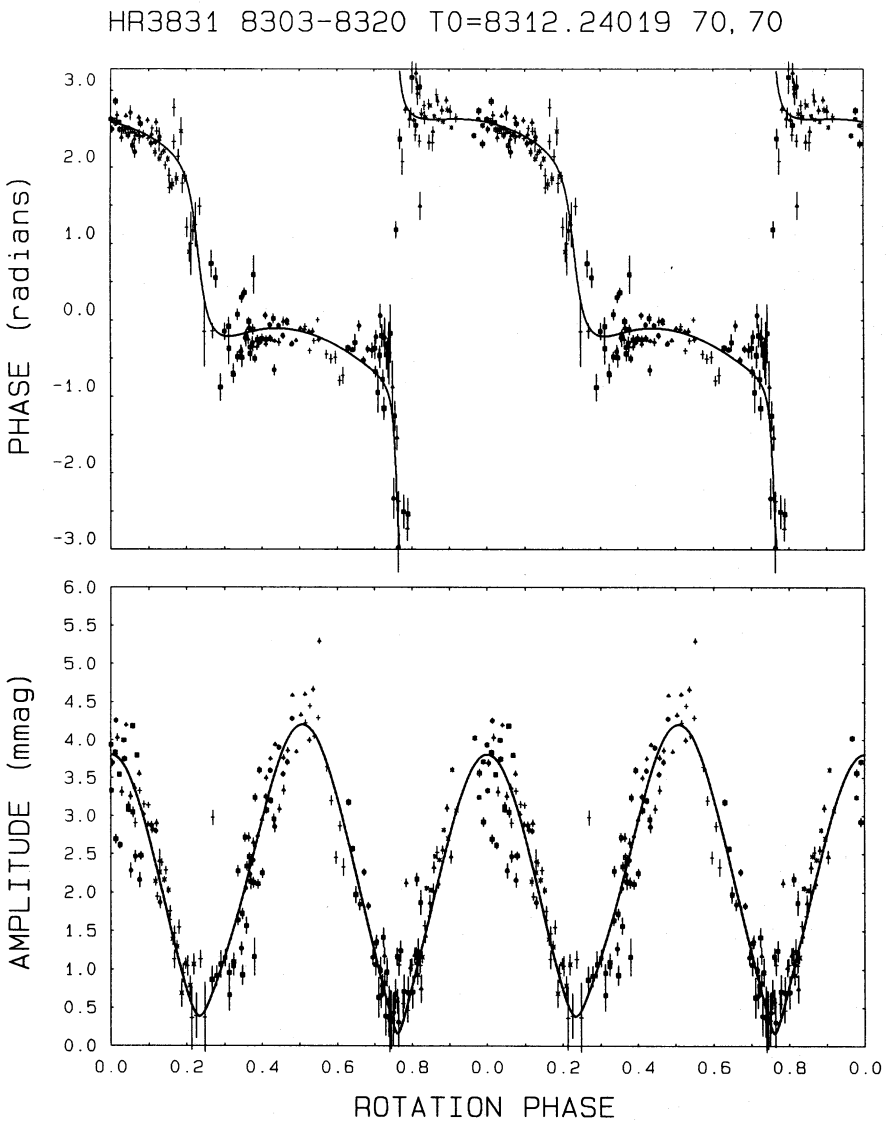

Figure 17. This diagram plots the pulsation phase and amplitude as a function of the rotation phase for the 1991 data. The rotation phase is calculated from the time of magnetic maximum using the ephemeris given by Kurtz et al. (1992) with the rotation period $P_{rot} = 2.851982$ d. Two rotation cycles are plotted. Each point in the diagram has been calculated by fitting the frequency $\nu = 1.4280128$ mHz to four cycles (46.685 min) of the high-speed photometric data by linear least-squares. The theoretical lines show the best fit to the low-frequency septuplet derived in Section 3 assuming a pulsation mode which can be described by the sum of $\ell = 0$, 1, 2 and 3 spherical harmonics. The components are given in Table 4 assuming a rotational inclination of $i = 70°$ and a magnetic obliquity of $\beta = 70°$. Data from JD 2448316 have been suppressed in this plot because of high noise caused by some light cirrus cloud on that night. This does not affect the solution, and it makes the comparison of the fitted curves and data points easier. For comparison, Fig. 3 shows the same data with JD 2448316 included.

over the time-span of the data sets. It does appear that the amplitude of $3\nu+\nu_{\rm rot}$ is greater than the amplitude of $3\nu-\nu_{\rm rot}$.

There is nothing to discuss about the third harmonic frequency except to reiterate that its detection at 4ν is probably significant.

5 INTERPRETATION

5.1 The low-frequency septuplet

Following the method described by Kurtz (1992), we have fitted a third-order axisymmetric spherical harmonic series to the frequency septuplet given in Table 2 for the fundamental frequencies. Table 4 shows the results of that fit for $i=70°$, $\beta=70°$. Most of the amplitude is in the dipole components, with smaller contributions from the radial, quadrupole and octupole components. We emphasize here that all of these modes are *not* excited – there is only one pulsation mode which is a distorted dipole described by $\ell=0$, 1, 2 and 3 components, e.g. as in Table 4.

There are few constraints on i and β for HR 3831. As we saw in the introduction, $i>38°$, either i or $\beta>62°$ and $i+\beta>90°$ because of the polarity reversal of the pulsation phase and magnetic field. Otherwise, i and β are unconstrained. However, the relative contributions of the $\ell=0$, 1, 2 and 3 components (as shown in Table 4) are strongly dependent on i and β, and many otherwise permissible values of i and β imply amplitudes for the components too large to be credible. Future work will explore the range of reasonable solutions.

Fig. 17 shows the pulsation amplitude and phase variation as a function of rotational phase for the 1991 data. The theoretical lines are constructed from the $\ell=0$, 1, 2 and 3 components given in Table 4 by the method given by Kurtz (1992). It is important to note that the fitted curves do not depend on i and β; the relative contributions of the $\ell=0$, 1, 2 and 3 components do, but the curve calculated from their

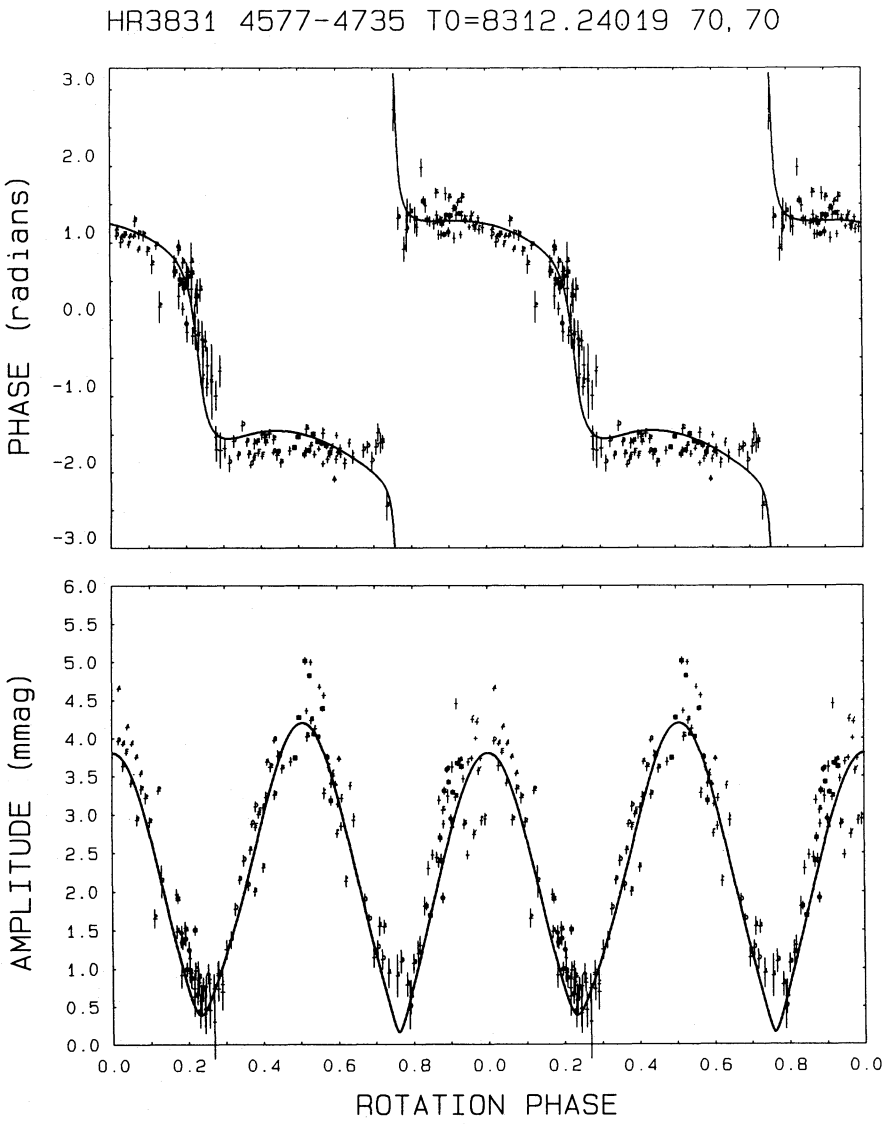

Figure 18. This diagram plots the pulsation phase and amplitude as a function of the rotation phase for the 1981 data. The fitted curves are from the 1991 data and hence are the same as those in Fig. 17, which are constructed from the components given in Table 4. The phase curve has been adjusted vertically to minimize the residuals to the fit.

correctly phased sum does not. This is, of course, because these components have been derived (assuming i and β) to give the best fit to the data points.

Fig. 3 showed the fit of a mode constructed of only $\ell = 0$ and 1 components. Comparison with Fig. 17 shows how much better the fit is when $\ell = 0$, 1, 2 and 3 components are included. The phase transition at the $\Theta = 0.253$ quadrature is well defined because the amplitude does not go to zero. The phase transition at $\Theta = 0.747$ is not well defined, possibly because the amplitude does go close to zero. We do not lack observations at this phase, but phase points with errors of 1 radian or more (which occur when the amplitude does go to zero) have been suppressed in the plot.

It appears that the phase transition at $\Theta = 0.747$ usually follows the fitted line, but can appear to go the other way. That is, the transition is usually in the negative-going direction, but can be in the positive-going direction. Comparison with Fig. 3 shows that the negative-going transition of the theoretical curve of Fig. 17 fits the data better than the positive-going transition of the $\ell = 0$ and 1 fit shown in Fig. 3.

Is this apparent uncertainty in the transition direction at the $\Theta = 0.747$ quadrature a numerical problem, or is it a physical effect in the star? As the pulsation amplitude approaches zero, the phase becomes poorly defined. The data points are calculated from lengths of the light curve only 47 min long, for which statistical deviations caused by sky transparency variations are more severe than for the longer light curves used in the frequency analysis. This might be all there is to the problem.

Remember that in the oblique pulsator model the true amplitude of the pulsation in HR 3831 is assumed not to vary with rotation – the observed amplitude varies because of the variable viewing aspect. As the observed amplitude approaches zero, the pulsation amplitude of one hemisphere cancels that of the other, since they are π radians out of phase with each other. If there is any small intrinsic instability in the true pulsation amplitude which may differ between the

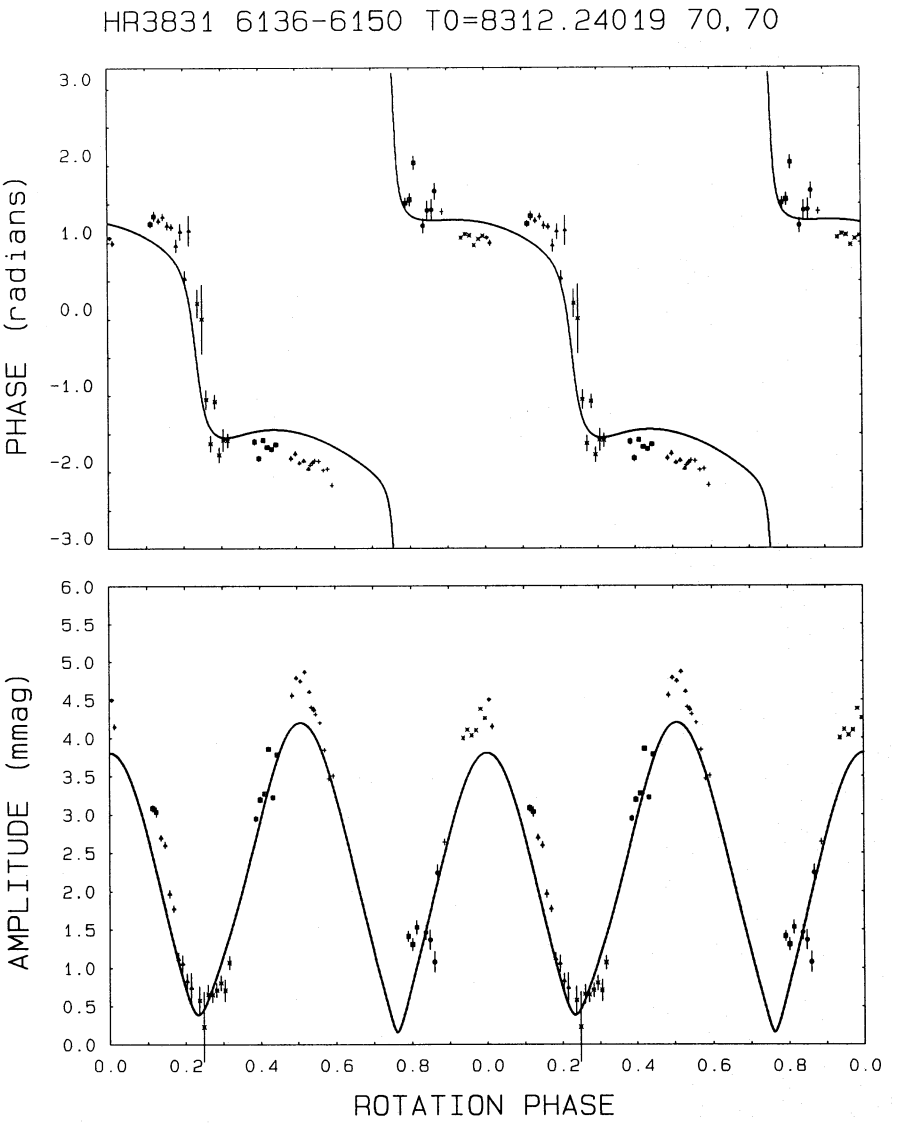

Figure 19. This diagram plots the pulsation phase and amplitude as a function of the rotation phase for the 1985 data. See caption to Fig. 18 for details.

hemispheres (and at *some* level, there must be), then the star may actually make the phase transition in different directions during different rotation cycles. The choice of direction in this case is probably stochastic.

We cannot yet distinguish between these two possibilities. Further analysis and statistical simulation are needed.

5.2 Long-term behaviour

The 1991 data set is the best data set we have for HR 3831. We therefore fit the theoretical amplitude and phase curves defined by the components given in Table 4 to other data sets to examine the long time-scale variability of those parameters. Figs 18, 19, 20 and 21 show the same theoretical curve as Fig. 17 fitted to the JD 2444577–4735, JD 2446136–6150, JD 2446501–6514 and JD 2447931–7963 data sets, respectively.

There appear to be real changes from year to year in the match of the fitted curves to the data, but some care needs to be taken in drawing this conclusion. For the JD 2446136–6150 (1985) data in Fig. 19, the points do not fit the curve precisely, but examination of Fig. 17 shows that the deviations are not much greater than the range shown in the more extensive 1991 data set. We take the year-to-year variability shown in Figs 18–21 to support our contention in Section 3, based on Table 3, that there are probably small but real changes in the light curves from year to year. In the context of the direction of the $\Theta = 0.747$ phase transition, it is interesting to note the positive-going transition direction for the 1986 data shown in Fig. 20.

Also noticeable in Figs 18–21 is the fact that the zero-point of the phase curve is different for the various data sets. This, of course, could be because the frequency fitted, $\nu = 1.4280128$ mHz, does not have a sufficient number of significant figures to phase all of the data sets together, or because the correct frequency is an alias of the fitted frequency; but this is not the case. That there is no single frequency which will phase all the data is shown by an analy-

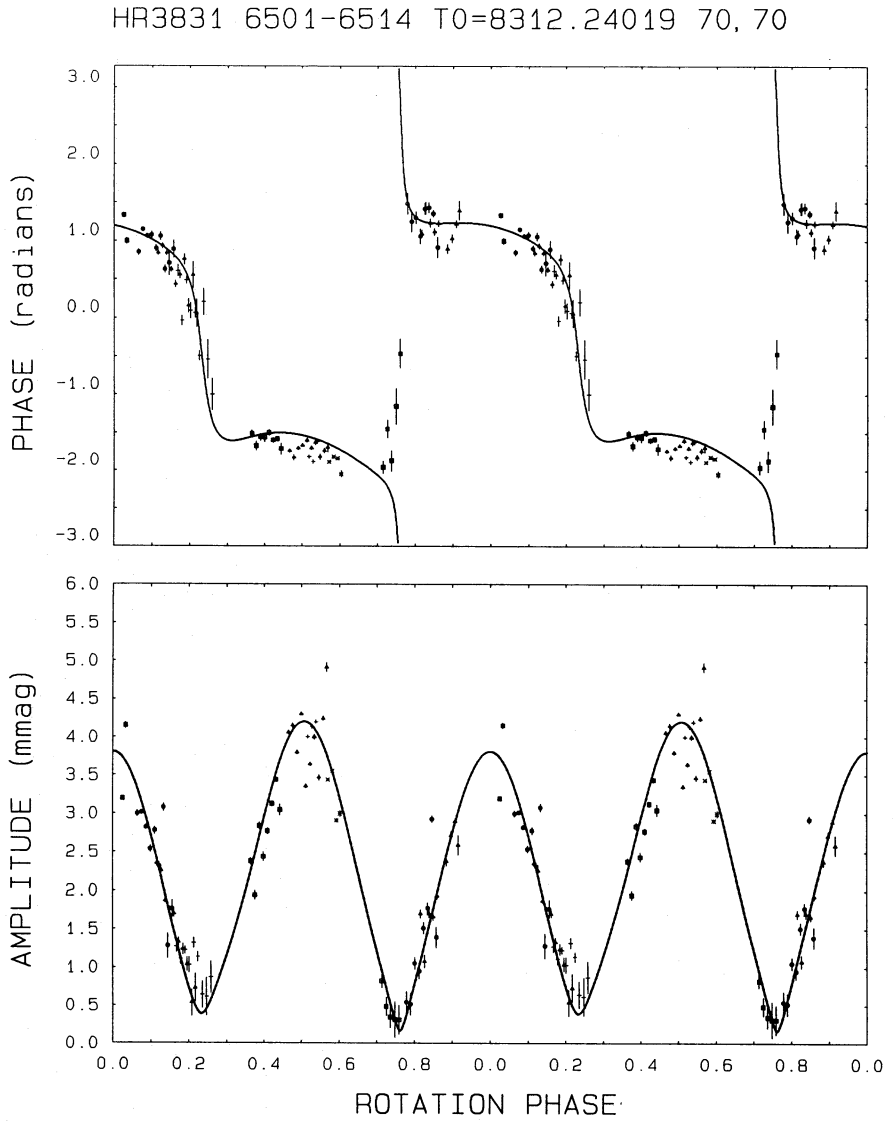

Figure 20. This diagram plots the pulsation phase and amplitude as a function of the rotation phase for the 1986 data. See caption to Fig. 18 for details.

sis of all of the HR 3831 data from 1981 to 1991 together. In that analysis, the highest peak in the amplitude spectrum lies near $\nu - \nu_{rot}$ (as it does in the individual, yearly data sets), but it has an amplitude of only 1.55 mmag. Examination of Fig. 15 and Table 4 shows that this frequency always has an amplitude near 2.0 mmag in the individual, yearly data sets. No frequency with this amplitude can be found in the entire data set because the phase of the pulsation is not constant. This inconstancy of the phase is illustrated in Figs 18–21, but its proof comes from the amplitude spectrum of the entire 1981–91 data set.

This phase inconstancy could be due in part to a Doppler shift caused by the orbit of HR 3831 about a companion, either seen or unseen. As we pointed out in the introduction, even the visual companion might produce a measurable effect with our 10 yr of data. It could also be due to evolutionary changes in the pulsation frequency. Heller & Kawaler (1988) have predicted that such changes should be measurable in roAp stars with 10 yr of data.

Another possibility is that the phase inconstancy is due to stochastic variability of the pulsation phase. In order to explain the locking of the pulsation and magnetic poles, Dolez & Gough (1982) suggested that the growth rates for the pulsation modes in roAp stars are short compared to the beat time of rotationally perturbed *m*-modes. Their idea was that modes would drift into and out of alignment with the magnetic field, and that only those aligned with the field would grow to observable amplitude. We think that the magnetic perturbation is sufficient to maintain the alignment of the pulsation and magnetic axes, but Dolez & Gough's suggestion does imply an unstable pulsation phase.

Fig. 22 is an O−C diagram for the pulsation phase of HR 3831. We have not yet been able to find a combination of Doppler shift and evolutionary change which can explain this diagram. Fig. 23 shows higher resolution O−C diagrams for the individual years; i.e. they are blow-ups of sections of Fig. 22. The top panel of Fig. 23 for the 1981 data shows either a quadratic curvature indicative of evolutionary

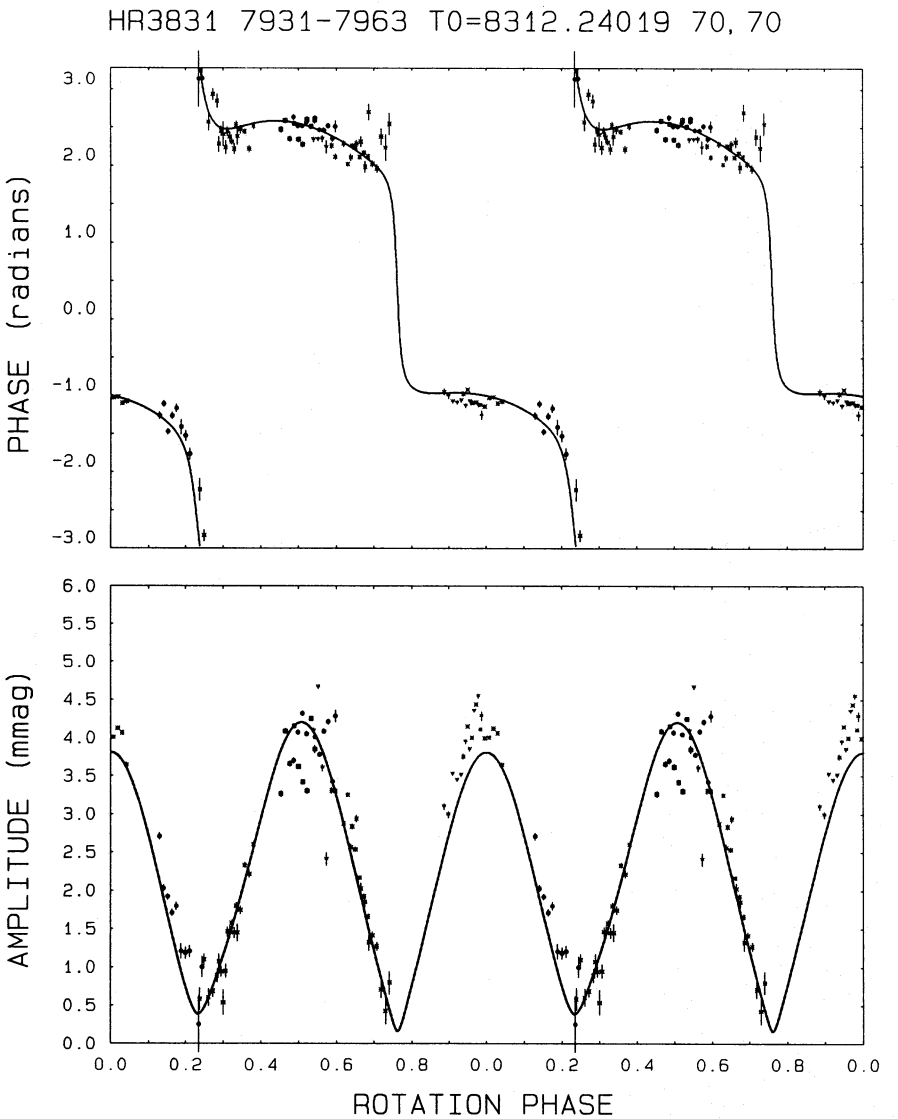

Figure 21. The diagram plots the pulsation phase and amplitude as a function of the rotation phase for the 1990 data. See caption to Fig. 18 for details.

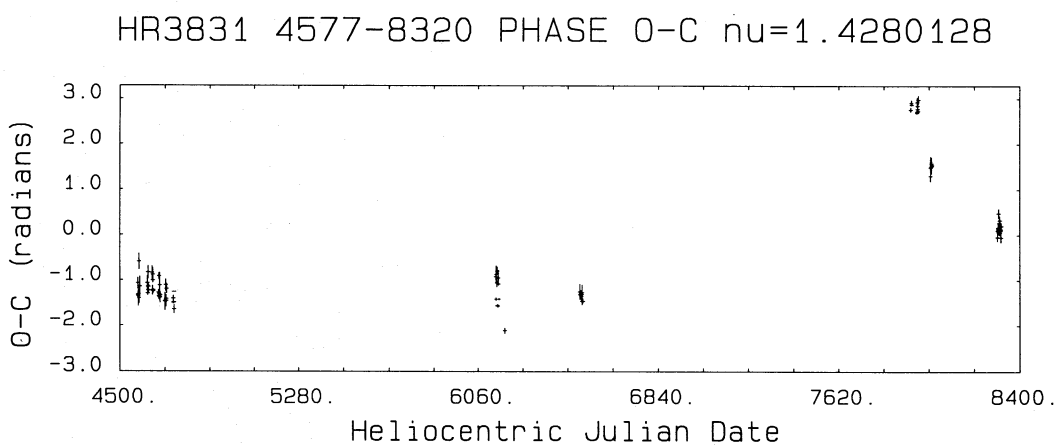

Figure 22. The pulsation phase O − C diagram. The ordinate value of each point is the phase shift necessary to bring the 1991 theoretical phase curve shown in Fig. 17 into agreement with the four-cycle linear least-squares phases for one night of data. This phase shift can be seen in the fit of the 1991 curve to the yearly data sets in Figs 18–21, but here each point represents just one night.

change (albeit on a very short time-scale), or a piece of a period curve indicative of a Doppler shift.

The points in the second panel are either flat, except for the JD 2446175 point on the right, or they have a linear slope indicating that the wrong frequency has been used. The third and bottom panels are flat, indicating the correct frequency, but they do not have the same zero-point. The fourth panel is flat for the JD 2447931–7963 data (although again with a large zero-point difference compared to the 1991 data in the bottom panel), but the points on the right for the JD 2448016–8024 data (see Table 1) are shifted in phase by about 1 radian (111 s!) with respect to the JD 2447931–7963 data.

The JD 2448016–8024 data were obtained over 2 weeks with two different telescopes at Sutherland. The observatory clock at Sutherland is checked weekly and kept accurate to a few tens of milliseconds. Cross-checks with another observer during that period show that there was no clock error. The phase difference in the fourth panel of Fig. 23 between the JD 2447931–7963 data and the JD 2448016–8024 data appears to be real. Note that this is similar in magnitude to the discrepancy of the JD 2446175 phase in the second panel.

This leads us to suggest that the pulsation phase in HR 3831 is not strictly periodic. To test this suggestion, short observing runs obtained frequently are needed. We are beginning a long-term monitoring of the pulsation phase of HR 3831 by obtaining a 1-h high-speed photometric light curve once per night at every opportunity through a Johnson *B* filter. In the past, observations of this star have been obtained intensively over a short time-span to study the frequency spectrum. Now needed are short light curves obtained frequently over a long time-span. The fitting of the theoretical phase curve, as in Figs 17–21, allows a unique phase shift to be determined for any light curve. Any high-speed Johnson *B* observations of this star of good photometric quality are useful for this programme, so all interested observers are encouraged to participate.

It was the inconstancy of the phase from year to year which gave rise to the additional frequencies which KSG (1990) found in their analysis of the 1981–86 data as a single data set. We find similar frequencies in an analysis of all of the 1981–91 data; they serve to modulate the phase of the frequencies in the observed septuplet, but not the amplitude.

5.3 The first harmonic quintet

KSG (1990) discussed the problem of the first harmonic frequencies. For the 1981–86 data, they found a frequency triplet with the amplitudes of the $2\nu - 2\nu_{\rm rot}$ and $2\nu + 2\nu_{\rm rot}$ frequencies equal to 0.20 mmag and the amplitude of the central 2ν frequency equal to 0.40 mmag; all three frequencies had the same phase; the $2\nu - \nu_{\rm rot}$ and $2\nu + \nu_{\rm rot}$ components of the presumed frequency quintuplet were unobserved. This means that the first harmonic frequencies were at maximum amplitude twice per cycle at the same time as were the fundamental frequencies, but with the same pulsation phase at both maxima, and they went to zero at quadrature. KSG could not understand this, because the first harmonic frequencies should behave as the square of the fundamental. With a dipole fundamental mode, they expected the harmonics to have a $\cos^2\theta$ surface distortion, which does not give zero amplitude when viewed at quadrature.

This problem is easily solved within the context of the spherical harmonic series description of the pulsation given in this paper. The square of the radial component of the fundamental could be of sufficient amplitude to account for the equality of the phases of the observed frequency triplet. Assuming that the fundamental was a pure dipole led KSG to expect that the central frequency should be π radians out of phase with respect to the $2\nu - 2\nu_{\rm rot}$ and $2\nu + 2\nu_{\rm rot}$ frequencies.

It has not yet been determined whether there is a choice of i and β which gives a spherical harmonic series description of the fundamental frequency septuplet which, when squared, is an adequate description of the first harmonic quintuplet. This problem has been complicated by the apparent changes in the first harmonic frequency quintuplet amplitudes from year to year (see Table 4 and Fig. 16).

5.4 The second harmonic frequencies

KSG (1990) found only one frequency, $3\nu + \nu_{\rm rot}$, at the second harmonic. In the 1991 data, we found $3\nu + \nu_{\rm rot}$ and

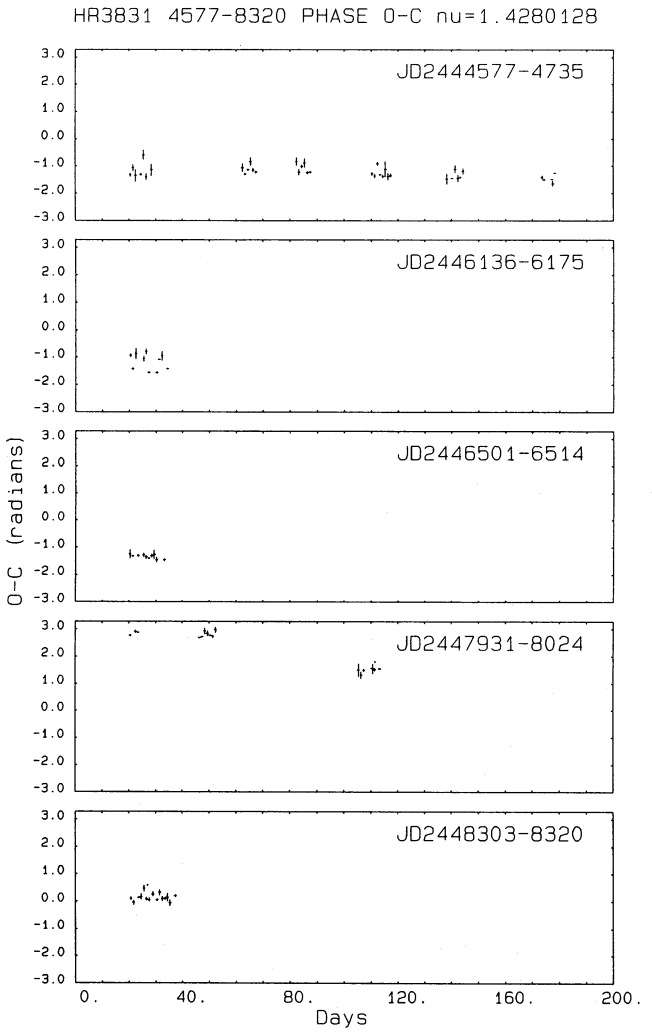

Figure 23. The phase O − C diagrams for the yearly data sets. Each panel is a blow-up of a section of Fig. 22. The top panel is for the 1981 data; the second panel is for the 1985 data - note that it includes the night of JD 2446175, which was not plotted in Fig. 19 because of its large O − C; the third panel is for the 1986 data; the fourth panel is for the 1990 data - note that it includes the nights of JD 2448016-8024, which were not plotted in Fig. 19 because of their large O − C; and the bottom panel is for the 1991 data. All panels are plotted to the same scale in both coordinates. The 1991 data are flat about O − C = 0 because the fitted frequency $\nu = 1.4280128$ mHz was derived from those data, as was the theoretical curve in Fig. 17 which defines the zero-point of the O − C scale. A frequency analysis of all of the data represented in Figs 22 and 23 shows that no single frequency can explain the variance in these diagrams; i.e. there is no alias of the selected frequency which would cause the O − C points only to scatter about zero.

$3\nu - \nu_{\rm rot}$, with the amplitude of the former slightly greater. This is still a surprise, as it was to KSG. Within the oblique pulsator model and the assumption of a pulsation mode which can be described by a summation of *axisymmetric* spherical harmonics, the amplitude of $3\nu + \nu_{\rm rot}$ cannot be greater than the amplitude of $3\nu - \nu_{\rm rot}$ for the (presumed) second harmonic triplet.

ACKNOWLEDGMENTS

DWK and PM acknowledge financial support from the Foundation for Research Development of the CSIR. We thank Mr Peter Tripe for obtaining the JD 2448016-8018 observations.

REFERENCES

Carney B. W., Peterson R. C., 1985, MNRAS, 212, 33P
Crawford D. L., 1979, AJ, 84, 1858
Deeming T. J., 1975, Ap&SS, 36, 137
Dolez N., Gough D. O., 1982, in Cox J. P., Hansen C. J., eds, Pulsations in Classical and Cataclysmic Variables. JILA, Boulder, p. 248
Dziembowski W., Goode P. R., 1985, ApJ, 296, L27
Heller C. H., Kawaler S. D., 1988, ApJ, 329, L43
Hoffleit D., Jaschek C., 1982, Bright Star Catalogue, 4th edn. Yale University Observatory, New Haven
Horne J. H., Baliunas S. L., 1986, ApJ, 302, 757
Houk N., 1978, Michigan Spectral Catalogue, vol. 2. Department of Astronomy, University of Michigan, Ann Arbor
Hurly P. R., Warner B., 1983, MNRAS, 202, 761
Kurtz D. W., 1982, MNRAS, 200, 807
Kurtz D. W., 1985, MNRAS, 213, 773
Kurtz D. W., 1990, ARA&A, 28, 607
Kurtz D. W., 1992, MNRAS, 259, 700
Kurtz D. W., Shibahashi H., 1986, MNRAS, 223, 557
Kurtz D. W., Shibahashi H., Goode P. R., 1990, MNRAS, 247, 558
Kurtz D. W., Kanaan A., Martinez P., Tripe P., 1992, MNRAS, 255, 289
Matthews J., 1991, PASP, 103, 5
Matthews J. M., Wehlau W. H., Walker G. A. H., Yang S., 1988, ApJ, 324, 1099
Mathys G., 1985, A&A, 151, 315
Mathys G., 1991, A&AS, 89, 121
Moon T. T., Dworetsky M., 1985, MNRAS, 217, 305
O'Donoghue D., 1981, Ph. D. Thesis, Univ. Cape Town, South Africa
O'Donoghue D., Warner B., 1982, MNRAS, 200, 563
Shibahashi H., 1986, in Osaki Y., ed., Hydrodynamic and Magneto-hydrodynamic Problems in the Sun and Stars. Dept. of Astron., Univ. Tokyo, Tokyo, p. 195
Shibahashi H., 1987, in Cox A. N., Sparks W. N., Starrfield S. G., eds, Stellar Pulsation. Lect. Notes Phys., Vol. 274, Springer-Verlag, Berlin, p. 112
Thompson I. B., 1983, MNRAS, 205, 43P